O-glycosylation regulates plant developmental transitions downstream of miR156

Krishna Vasant Mutanwad[1], Alexandra Baekelandt[2,3], Nicole Neumayer[1], Claudia Freitag[1], Isabella Zangl[1], Dirk Inzé[2,3] and Doris Lucyshyn[1*]

[1]Department of Applied Genetics and Cell Biology, University of Natural Resources and Life Sciences, Vienna, Muthgasse 18 1190 Vienna, Austria.
[2]Ghent University, Department of Plant Biotechnology and Bioinformatics, Technologiepark 71, 9052 Ghent, Belgium.
[3]VIB Center for Plant Systems Biology, Technologiepark 71, 9052 Ghent, Belgium.

[*]Correspondence: doris.lucyshyn@boku.ac.at

Keywords: *Arabidopsis thaliana*, O-glycosylation, plant development, phase change, flowering time, SPL

SUMMARY

The timing of plant developmental transitions is decisive for reproductive success and thus tightly regulated. The transition from juvenile to adult vegetative and later to the reproductive phase is controlled by an endogenous pathway regulated by miR156, targeting the SQUAMOSA PROMOTER BINDING PROTEIN (SBP/SPL) family of transcription factors. SPLs regulate a number of developmental processes, such as trichome formation, leaf shape and floral transition. Such complex regulatory pathways often involve post-translational modifications (PTMs), integrating a range of internal and external signals. One of these PTMs is O-glycosylation, the attachment of a single monosaccharide to serine or threonine of nuclear and cytoplasmic proteins, which is found on a number of very diverse proteins. O-GlcNAcylation is the most common type of cytosolic O-glycosylation, but in plants also O-fucose modification occurs. Here we show that mutants defective in the O-fucosyltransferase SPINDLY (SPY) show accelerated developmental transitions. Genetic analysis shows that this effect is independent of miR156 levels, but partly dependent on functional SPLs. In a phenotyping analysis, we found that SPY and SPLs also control leaf growth, as loss of function mutants showed defects in cell expansion, while SPL9 also regulates cell division in rosette leaves. Moreover, SPLs interact directly with SPY and are O-glycosylated. Our results show that O-glycosylation is involved at several steps in the regulation of developmental transitions and organ growth in *Arabidopsis thaliana*.

INTRODUCTION

During their life cycle, plants undergo developmental transitions by changing from the juvenile to adult vegetative and later the reproductive phase [1-3]. Each of these irreversible transitions is marked by specific morphological and developmental changes, and while they are governed by an internal developmental program, the timing is flexible and can be influenced by the environment. Both of these phase transitions are controlled by small RNAs, the families of miR156 and miR172. miR156 is encoded by eight genes, and there is at least partial redundancy with the closely related miR157, which is encoded by four genes [4]. miR156 directly targets a group of transcription factors within the family of SQUAMOSA PROMOTER BINDING PROTEINs (SBP/SPL), which then control both transitions by inducing a number of transcription factors regulating adult leaf traits, floral transition and floral meristem identity, as well as the expression of miR172 [5-14]. The family of SPLs contains 16 members, but only

well as the expression of miR172 [5-14]. The family of SPLs contains 16 members, but only 10 of them are targeted by miR156. Interestingly, regulation occurs both by transcript cleavage as well as translation repression, reflecting the high level of complexity in the regulatory pathways of developmental transitions [4, 15]. Additionally, the decrease in miR156 expression throughout development is strongly influenced by metabolism: the accumulation of sugars during plant growth leads to a decrease in miR156 and thus an increase in miR172, which then additionally feeds back negatively on the expression of miR156 [16, 17]. Thereby as plants grow and build up biomass, the increasing availability of sugars leads to a release of the repression of SPL transcription factors and thus the developmental switch from the juvenile to adult and later reproductive phase. At the same time, organ growth is promoted by a transition from the proliferative phase characterized by cell divisions, to a phase where cell expansion is driving growth. This is regulated by GROWTH-REGULATING FACTORs (GRFs), a group of transcription factors regulated by miR396 [18-20]

The timing of transitions is extremely important for plants to ensure reproductive success. Thus, the transition from the vegetative to the reproductive phase is controlled not only by the internal developmental program described above, but also by seasonal cues and environmental conditions, such as day length, ambient temperature or light quality, which are integrated at several levels. Environmental factors, most importantly day length, are perceived in the leaves, where they induce the expression of the floral integrator *FLOWERING LOCUS T* (*FT*). FT is a small, mobile protein, moving through the vasculature to the shoot apical meristem, where it interacts with the transcription factor FLOWERING LOCUS D (FD) to induce flowering [21-23]. In the shoot apical meristem, the floral integrators SOC1 (SUPRESSOR OF OVEREXPRESSION OF CONSTANTS 1), LFY (LEAFY) and FT regulate the transcriptional network that underlies flowering time control, as reviewed in [24]. A role for gibberellins (GAs) in the induction of flowering time has already been suggested in the 1950s [25, 26], and research on the long-day plant *Arabidopsis thaliana* has shown that GA is necessary for floral induction under short photoperiods [27]; In long days, its effect is mostly masked by the much earlier responding photoperiod pathway [28]. Gibberellins have since been placed at several points within the flowering time regulatory network [11-13, 29-33], with *SOC1*, *LFY* and/or *SPLs* being direct targets. The effect of GA on flowering time is mediated by DELLA proteins, a small family of five transcriptional repressors that are negatively regulated by GA [34]. In the absence of GA, DELLA proteins bind to a number of transcription factors, thereby preventing their ability to bind their target genes [35-37]. The miR156-regulated aging pathway is independent of photoperiod, but is affected by gibberellins, as SPL15 is directly inhibited by the interaction with the DELLA protein RGA in the absence of GA [12].

O-glycosylation of nucleocytoplasmic proteins is an abundant post-translational modification, with diverse targets. In plants, two O-glycosyltransferases are described in this context, the O-GlcNAc Transferase (OGT) SECRET AGENT (SEC) and the Protein O-Fucosyltransferase (POFUT) SPINDLY (SPY) [38, 39]. These enzymes use UDP-GlcNAc (N-acetylglucosamine) and GDP-fucose, respectively, to transfer the single sugar moiety to serine or threonine residues on their target proteins. Among these targets are the GA signaling-repressing DELLA proteins as well as a number of other transcriptional regulators [38-40]. So far, only few examples of regulation by O-glycosylation have been characterized in plants. While *sec*-mutants show only very subtle phenotypes, *spy*-mutants show a range of developmental defects, and most of them have been explained by enhanced GA signaling [38, 39, 41-43]. One of the most prominent features of *spy*-mutants is early flowering. In long photoperiods, SPY acts together with GIGANTEA (GI) to repress expression of *CONSTANS*

(*CO*) and *FT* [44]. SPY also strongly represses flowering in short photoperiods, which has been explained by its role in regulating GA signaling [41, 42].

Here, we present a further characterization of the role of SPY in the control of floral transitions and show an additional function of O-glycosylation in the regulation of the transition from juvenile to adult vegetative, and then to the reproductive phase. A combination of genetic and phenotypic analysis suggests a direct regulation of SPL-transcription factors downstream of miR156 by O-glycosylation. We also observed that leaf growth is strongly affected by SPY and SPLs at the level of cell expansion. While there was also an effect of SPL9 on cell division, we did not see an indication for control of cell division by glycosylation. We describe effects of protein O-glycosylation that are potentially independent of gibberellins, with redundancy between O-GlcNAc and O-fucose modification, but a much stronger effect of O-fucosylation.

RESULTS

The O-fucosyltransferase SPINDLY delays flowering in long and short photoperiods

In order to characterize the effect of O-glycosylation on flowering time regulation, we studied flowering time in O-glycosylation mutants. As strong *spy* alleles show severely reduced fertility [39, 41], we used the T-DNA-insertion line *spy-22* (SALK_090582) for all our experiments. This line showed strongly reduced expression of SPY (Fig.S1A-B) and was flowering early at 8.6 ±1.4 total rosette leaves (TRL), compared to 13.1 ± 1.1 in the wild-type Col-0 (Figure 1A-B, Table 1). The early flowering of *spy-22* was complemented by a *SPY::SPY:Flag* (*SPY:Flag*) construct (Fig.S1C-D). Recently, modest early flowering of *sec-5* was reported [45], which we also observed, with a very small difference to the wild-type (11.8 ± 1.6 TRL in *sec-5* compared to 13.1 ± 1.1 in Col-0; Figure 1A-B, Table 1). Accordingly, expression of the major floral integrator gene *FT* was up-regulated in *spy-22* but not *sec-5*, (Figure 1C). When grown in short photoperiods (8 h light / 16 h dark), where *FT* is not expressed, *spy-22* also displayed strong early flowering with 22.7 ± 0.5 TRL compared to 66.0 ± 7.9 in Col-0, which we did not observe in *sec-5*, flowering at 61 ± 5.0 TRL (Figure 1D-E, Table 1). Early flowering of *spy-22* was only partially suppressed by *ft-10*, resulting in a phenotype of *ft-10 spy-22* (17.4 ± 1.4 TRL) intermediate between *ft-10* (47.7 ± 2.9 TRL) and the wild-type Col-0 (14.6 ± 1.3 TRL), while *ft-10 sec-5* (46.2 ± 6.4 TRL) was comparable to *ft-10* (Figure 1F, Table 1). This confirms previously shown results with mutants in the L*er*-0 background [44], indicating that SPY regulates flowering by regulating *FT* and additionally in an *FT*-independent manner. This suggests that additional factors independent of the photoperiod pathway may be affected by SPY, while SEC appears to play a minor role. Therefore, we also generated crosses with the late flowering Col-0 FRI. This line carries an active FRIGIDA (FRI) allele introgressed from the ecotype Sf-2, and consequently expresses high levels of the floral repressor *FLOWERING LOCUS C* (*FLC*) leading to very low levels of *FT* expression and requirement of vernalization for floral induction [46, 47]. Late flowering of Col-0 FRI (74.2 ± 7.8 TRL) was strongly accelerated in *spy-22* FRI (26.0 ± 1.4 TRL, Figure 1G), but it was not affected by *sec-5* (data not shown). Levels of *FLC* expression were maintained high in that line, and *FT* was repressed (Figure 1H), suggesting that SPY represses flowering in Col-0 FRI independently and in addition of the vernalization pathway and FT. Thus, our data indicate that SPY represses floral transition only partly via FT and the photoperiod pathway. Additionally, SPY is necessary to maintain the vernalization requirement of Col-0 FRI.

143 **Mutants in SPY show accelerated transition from juvenile to adult phase**

144 Bypassing of the vernalization requirement of Col-0 FRI has previously been shown in
145 lines expressing an miRNA-resistant stabilized version of SQUAMOSA PROMOTOR-
146 BINDING PROTEIN-LIKE 3 (rSPL3) that lacks an miRNA-binding site [9]. SPL-transcription
147 factors regulate the juvenile to adult vegetative phase transition as well as flowering time; thus,
148 we analyzed also the juvenile to adult vegetative phase change in O-glycosylation mutants.
149 This transition is morphologically marked by the formation of trichomes on the abaxial side of
150 leaves and changes in leaf morphology, an increase in the ratio of length to width of leaf
151 blades, and the onset of serration [48] [49]. Based upon appearance of trichomes on the
152 abaxial side of rosette leaves, we observed that *spy-22* plants consistently transitioned early
153 from the juvenile to the adult stage at 3.5 ± 0.6 juvenile leaves (JL) compared to 5.8 ± 0.6 JL
154 in Col-0, while *sec-5* (5.9 ± 0.7 JL) did not show significant differences compared to the wild-
155 type (Figure 2A, Table 2). In order to dissect the juvenile to adult phase transition from floral
156 transition, we included *ft-10-spy-22* in this analysis. We found that *ft-10* had a delayed juvenile-
157 to-adult transition, with 9.2 ± 1.0 JL, which had been shown before [50]. On the other hand, *ft-*
158 *10 spy-22* was similar to *spy-22* with 3.5 ± 0.6 JL, even though *ft-10 spy-22* (17.4 ± 1.3 TRL)
159 showed an extended adult vegetative phase and was flowering considerably later than *spy-*
160 *22* (7.1 ± 0.6 TRL) (Figure 2B, Table 2). This suggests that phase transition is regulated
161 independently of daylength-dependent flowering time in *spy-22*. Juvenile-to-adult phase
162 transition is regulated by an internal developmental program, orchestrated by a balance of
163 counteracting miR156 and miR172 [7, 51]. Thus, we analyzed transcript levels of primary
164 miRNA156a, miRNA156b and miRNA156c in 5-day old seedlings, but did not find differences
165 between the wild-type and *spy-22* (Figure 2C).

166 Levels of miR156 are, among other pathways, regulated by the accumulation of sugars
167 in the leaves of growing plants [16, 17]. Cellular nutrient availability, especially increased sugar
168 levels, enhance global levels of O-glycosylation in animals [52-55]. To test if O-glycosylation
169 might be involved in regulation of miR156 abundance in response to sugar levels in plants,
170 we treated 5-day old Col-0, *spy-22* and *sec-5* seedlings with 50 mM sucrose by transferring
171 them to liquid media with and without added sucrose for 24 h. While we could reproduce the
172 results of a strong decrease in miR156a, miR156b and miR156c in response to sucrose
173 treatment as shown before [16, 17], we did not see any significant differences between *spy-*
174 *22* and the wild-type after the treatment (Figure 2D).

175 We then compared expression of mature miR156 and miR172 in juvenile and adult
176 leaves of soil-grown plants. Leaves were harvested for all lines at the timepoint when the wild-
177 type plants started to bolt. We observed balanced levels of miR156 and miR172 between
178 juvenile and adult leaves in Col-0. *spy-22*, which was already flowering, showed a strong shift
179 in the balance towards miR172, with a more than 4-fold increase in adult leaves compared to
180 the juvenile leaves (Figure 2E). *sec-5* showed the same tendency, but at a lower level, while
181 *ft-10* and *ft-10 spy-22*, which were not flowering yet when the samples were taken, showed
182 lower levels of miR172 in adult compared to juvenile leaves (Figure 2E). This observation
183 correlates with the flowering time of these lines (Figure 1D and 2B, Table 1) and their
184 developmental stage at the timepoint of sampling, with miR172 levels being increased in the
185 lines that were already in the reproductive phase and decreased in the lines remaining in the
186 vegetative stage. We did not observe a change in the ratio of miR156 in juvenile leaves
187 compared to adult leaves in *spy-22* or *sec-5* in comparison to the wild-type (Figure 2E). We
188 repeatedly observed lower levels of miR156 in adult leaves of *ft-10*, but not in *ft-10 spy-22*,

again correlating with the fact that *ft-10* is the line with the longest vegetative phase in this dataset and was far from transition at the timepoint of sampling.

Taken together, we did not see a change in levels of miR156 in *spy-22* or *sec-5*, but we observed an increase in miR172 levels in *spy-22* and sec-5 as a consequence of accelerated floral transition. Our results suggest that there is no involvement of O-fucosylation in regulating the levels or balance of miR156 and miR172 during developmental phase transitions.

SPY regulates phase transitions via SPL transcription factors independently of miR156

To further test for a potential interaction between miR156 and O-glycosylation in the regulation of developmental transitions we generated *35S::MIRNA156a* lines. Overexpression of *miRNA156a* in Col-0 led to a strong delay of the juvenile-to-adult phase transition and extremely delayed flowering, as shown before [7, 9] (Figure 3A-D). We then crossed *35S::MIRNA156a* Col-0-with *spy-22* and *sec-5*, and the offspring of these crosses displayed a strong repression of the miR156 overexpression phenotype. While *35S::MIRNA156a* Col-0 formed 51.8 ± 6.8 leaves, *35S::MIRNA156a spy-22* was flowering at 9.2 ± 1.2 TRL and *35S::MIRNA156a sec-5* at 11.3 ±1.2 TRL (Figure 3 A - C). A comparison of expression levels of miR156 in juvenile leaves *35S::MIRNA156a spy-22* and *35S::MIRNA156a sec-5* with the respective parent lines *spy-22, sec-5, 35S::MIRNA156a* Col-0 and the wildtype Col-0 showed very high levels of mature miR156 in the crossed lines, with miR156 levels at the same level in *35S::MIRNA156a* Col-0 and *35S::MIRNA156a spy-22*, and weaker overexpression in *35S::MIRNA156a sec-5* (Figure 3D). These data show that the effect of overexpressing miR156 is strongly suppressed in both *spy-22* and *sec-5* and that the early flowering of these mutants is independent of miR156 levels.

miR156 targets the family of SPL-transcription factors, which induce juvenile and adult phase transitions and floral transition [4, 7, 8, 51]. We therefore generated crosses of the O-glycosylation mutants with *spl9-4 spl15-1*, a line displaying delayed phase change, to test if SPLs are necessary for early developmental transitions of *spy-22*. We chose this line, as it has been characterized to show the strongest effect in delaying phase transitions among combinations of *SPL*-double mutants previously described [8], and both SPL9 as well as SPL15 directly interact with the DELLA protein RGA [11, 12], which is itself a target of SPY and SEC [38, 39]. We included *SPL9::rSPL9:GFP* [9] in our analysis, a line carrying an miR resistant version of SPL9 that consequently displays very early phase transitions. The early juvenile-to-adult transition of *spy-22* (3.5 ± 0.6 JL) was partly suppressed in the *spy spl9/15* triple cross (5.4 ± 0.7 JL), and flowering time was also affected (7.8 ± 1.1 TRL in *spy-22,* and 10.2 ± 1.5 TRL in *spy spl9/15*, Figure 4A-B, Table 4). In *sec spl9/15*, the number of juvenile leaves was slightly increased compared to *sec-5* (5.9 ± 0.7 JL in *sec-5* and 6.8 ± 0.7 JL in *sec spl9/15*), and *spl9/15* also delayed flowering of *sec-5* in the triple mutant (11.4 ± 1.03 TRL in *sec-5* and 16.3 ± 1.5 TRL in *sec spl9/15*) indicating that SPY and SEC might have common functions in this pathway (Figure 4A-B, Table 4). We did not see a full suppression of the early flowering of *spy-22* in *spy spl9/15* to the level of *spl9-4/15-1*. SPLs are encoded by a gene family with partially overlapping functions [8, 15], and potentially higher order *SPL*-mutants could lead to a stronger effect. Also, the effect of SPY on the photoperiod pathway and *FT* expression function independently and in parallel to the aging pathway, accelerating flowering time in parallel to SPLs.

We also observed additive effects in shoot architecture in the triple crosses (Figure 4B). While *spy spl9/15* showed a strong loss of apical dominance compared to the wildtype, we observed the opposite in *sec spl9/15*, with a strong increase in apical dominance. While we

236 did not follow up or quantify these observations yet, this might be an indication that SPY and
237 SEC function redundantly as well as independently in different pathways.
238 We also observed the plastochron length by quantifying the number of leaves formed in
239 regular intervals in parallel to determining the absolute leaf number (Figure 4C-D).
240 *SPL9::rSPL9:GFP* was previously described as having a long plastochron, producing fewer
241 leaves per day than wildtype, while *spl9/15* has a short plastochron [9], which we also
242 observed. In this analysis, both *spy-22* and *sec-5* show a slightly longer plastochron compared
243 to the wildtype, which was suppressed in both triple crosses with *spl9/15* (Figure 4C-D).
244 Taken together, our results suggest that SPY and SEC both negatively regulate phase
245 change and flowering independently of miR156, potentially in interaction with SPLs.
246
247 **SPY and SPL9/15 are involved leaf size determination**
248 While quantifying flowering time of the distinct mutants, we noticed additional shoot growth
249 phenotypes that were not observed in the parent lines. In order to analyze these in more detail
250 and dissect putative additive effects, we determined individual leaf areas as well as rosette
251 areas and rosette growth rates (Figure 5). At 25 days after sowing (DAS), *spy-22* showed
252 strongly decreased leaf areas, while *sec-5* had only slightly smaller leaves (Figure 5A, B). The
253 *spl9/15* mutant had produced more leaves than the wildtype at this timepoint, correlating to
254 the shorter plastochron (Figure 4C and 4D). Additionally, *spl9/15* showed a strong decrease
255 in the areas of the first 7 leaves, while the leaf areas from leaf 9 onwards were increased
256 compared to the wild-type Col-0, suggesting a developmental shift. This shift was also
257 observed in the triple crosses with *spy-22* and *sec-5*. Additionally, we observed a clear additive
258 effect for the decrease in leaf size, suggesting that O-glycosylation and SPL9 and SPL15
259 regulate leaf size independently from each other, but the developmental shift seen in *spl9/15*
260 is epistatic in the triple crosses (Figure 5B). *SPL9::rSPL9:GFP* showed the highest increase
261 in leaf size (with leaf 1 and 2 showing an increase in leaf area of 121% compared to Col-0)
262 and a developmental shift compared to the wild-type in the opposite direction of *spl9/15*. Also
263 in contrary to *spl9/15*, the number of leaves produced in *SPL9::rSPL9:GFP* at 25 DAS was
264 strongly reduced to 3.9 ± 0.3 leaves, compared to 13.0 ± 1.0 leaves in the wildtype, similar to
265 the increased plastochron observed in (Figure 4C-D), and [9]. Accordingly, the rosette area
266 calculated as the sum of the individual leaf areas (mm^2) was drastically reduced in
267 *SPL9::rSPL9:GFP* (Figure 5A,C). At 25 DAS, *spy-22* and *spy-22 spl9/15* also showed a strong
268 reduction in rosette area, while rosettes of *sec-5* were only slightly reduced (Figure 5A-B). The
269 rosette areas of *spl9/15* and *sec spl9/15* were not significantly affected (Figure 5 A-C).
270 In a time course analysis, rosette growth correlated to the plastochron length in the
271 analyzed lines (Figure 4C and D), with *SPL9::rSPL9:GFP* showing the slowest growth (Figure
272 5C-D). This is mainly resulting from the low number of leaves, as the individual leaf size for
273 the first developing leaves was increased strongly in this line compared to Col-0 (Figure 5B).
274 In *spl9/15,* the decrease in leaf size (Figure 5B) was partly compensated by the higher number
275 of leaves due to shorter plastochron (Figure 4C and D). A positive correlation of plastochron
276 and leaf size has also previously been shown in [56]. *spy-22* and *spy spl9/15* showed a
277 considerably slower rosette growth compared to the wildtype, due to decreased leaf size. *sec-*
278 *5* and *sec spl9/15* showed rosette growth rates comparable to the wildtype (Figure 5D).
279 To determine the cellular effect of the differences in leaf areas observed in O-
280 glycosylation and *spl* mutants, we determined epidermal cell size and number in the first leaf
281 pair (L1/2) of all lines. Leaves were harvested at 25 DAS, a timepoint when wild-type Col-0
282 leaves are considered mature. The leaves were cleared and microscopic drawings of the cells
283 were used to determine pavement-, guard- and total cell number and individual pavement cell

area (Figure 6A). Total cell number (guard and pavement cells) was strongly increased in *SPL9::rSPL9:GFP* (Figure 6B, Fig. S2A-B), but there was no change in pavement cell area (Figure 6C), suggesting that the increase in leaf area in *rSPL9* mutants is due to increased cell division. In all other lines, guard- and pavement cell numbers were not significantly changed compared to the wildtype (Figure 6B, Fig. 6SA-B). When measuring individual pavement cell areas (PCA), we found a decrease in *spy-22* (-34%) and *spy spl9/15* (-47%) compared to the wild-type, with a clear additive effect. PCA was also decreased in *spl9/15* (-30%) and *sec spl9/16* (-23%) mutants, though not statistically significant. The measurements go in line with the decrease in leaf and rosette area described above, suggesting that the leaf area decrease in *spy-22*, *spl9/15* and *spy spl9/15* results from additive defects in cell expansion (Figure 5B). However, we cannot exclude that the observed effects are not due to slower leaf growth rates on cellular level in these lines. Analysis of mature leaves in *spy-22* and *spy spl9/15*, taking samples at a later timepoint, could further address this question. Overall, however, our data suggest that cell division is not affected in these mutants. Given the increased cell division in *SPL9::rSPL9:GFP* (Figure 6A-C), we cannot exclude that redundancy among SPLs masks potential effects on cell division in *spl9/15*. Analysis of higher order mutants would address this question.

The distribution of cell sizes indicates fewer cells in the category of the biggest cells in *spy-22*, and especially in *spy spl9/15* (Figure 6D), correlating with the results of the decreases in leaf area (Figure 5B). The number of cells in the smallest category is increased in these lines, suggesting a developmental shift at cellular level. Again, however, we cannot exclude that this is potentially due to cells not yet having reached maturity in these lines.

We then also determined stomatal index (SI) and stomata density (SD), corresponding to the proportion of stomata per pavement cells and the density of the stomata, respectively. For SI, we only observed a slight increase in *SPL9::rSPL9:GFP*, suggesting that more stomata are initiated, while all the other lines did not show significant differences compared with wildtype (Figure 6F). On the other hand, SD was significantly increased in *spy-22* and *spy spl9/15* (Figure 6G), likely to result from the decrease in average pavement cell area in these lines at the timepoint used for phenotypic analysis (Figure 6C).

Overall, our data suggest that SPL9 positively regulates cell division, while we did not see an effect on cell division in the other analyzed lines. We also observed a reduction in pavement cell area in *spy-22* and *spy spl9/15,* either due to defects in cell expansion or delayed growth rates.

SPY O-fucosylates SPL transcription factors

Several SPLs were recently shown to be O-GlcNAc modified, among them also SPL8, which does not carry a miR156 recognition site [40]. We therefore tested if SPL15, which is important for the control of flowering time, directly interacts with SPY and can be O-fucosylated. *35S::FLAG:SPY* was co-infiltrated with *35S::SPL15:HA* and *35S::SPL8:HA* as a positive control, respectively, in *N. benthamiana* leaves for co-immunoprecipitation. When analyzing protein expression after infiltration of *N. benthamiana* leaves, we could clearly see a shift of SPL8 and SPL15 when co-infiltrated with SPY compared to the independent infiltration, suggesting a modification of SPL8 and SPL15 by SPY (Figure 7A). Interestingly we also consistently observed a stabilization of SPL8 and SPL15 in the samples co-infiltrated with SPY compared to single infiltrations (Figure 7A, a representative example of several biological repeats is shown.) When precipitating Flag:SPY with an anti-Flag antibody, we could pull down SPL15, indicating protein-protein interaction (Figure 7B). These results indicate that

331 SPY directly interacts with, and glycosylates SPL15. Together with our data from genetic
332 analysis, this suggests that SPY inhibits SPL-activity by glycosylation.
333
334 **DISCUSSION**
335 A multitude of different post-translational modifications (PTMs) confer complexity to
336 the regulation of protein function and stability. They are essential components of signalling
337 pathways in the course of development, often integrating environmental changes or fine-
338 tuning crosstalk between different regulatory pathways. O-glycosylation of cytosolic and
339 nuclear proteins is the modification of a number of very diverse proteins with a single
340 monosaccharide on serine or threonine residues – which is in contrast to N-glycosylation
341 events that involve the formation of branched carbohydrate chains of varying composition in
342 the secretory pathway [57]. Most organisms carry only one type of cytosolic O-glycosylation,
343 with O-GlcNAcylation being the most common and best described example that is very well
344 conserved among all kingdoms. Yeast is lacking an O-GlcNAc transferase, but uses instead
345 O-mannose modification for the same molecular function. Many of the target proteins are
346 however conserved between yeast and animal cells [58, 59], suggesting that the molecular
347 function is more conserved than the type of monosaccharide involved. Plants are exceptional
348 in that they use two different sugars attached to the same protein targets [39]. Currently the
349 only other organism described to use fucosylation as well as GlcNAc modification is
350 *Toxoplasma gondii*, but probably with distinct targets for the two different modifications [59].
351 In Arabidopsis, only few O-glycosylated targets have been characterized so far. O-
352 glycosylation of the transcription factors TEOSINTE BRANCHED, CYCLOIDEA AND PCF 14
353 (TCP14) and TCP15 by SPY increases their stability during cytokinin signalling [60, 61]. SPY
354 was also implicated in the integration of reactive oxygen species signalling during root
355 development [62]. Further protein interactions between SPY and GIGANTEA [44], and SPY
356 and SWI3C [63] have been identified. However, by far the best characterised O-glycosylated
357 protein in plants is the DELLA protein RGA. The current model suggests that O-GlcNAc and
358 O-fucose modification have opposite effects on DELLAs during GA signalling, with O-
359 GlcNAcylation leading to a closed conformation of DELLAs, rendering them less active. On
360 the other hand, fucosylation leads to an open conformation of RGA, facilitating the interaction
361 with target transcription factors, thus increasing DELLA activity [38, 39]. However, a number
362 of open questions remain, even in the context of GA signalling, such as the observation that
363 the double knockout of SPY and SEC is embryonic lethal even using weaker alleles, while the
364 single mutants don't show drastic developmental phenotypes [64]. This suggests that there
365 might be targets where both modifications have the same effect, or even both modifications
366 are necessary at the same time, though not identified so far. A proteomic study using lectin
367 weak affinity chromatography (LWAC) with glucosamine-binding wheat germ agglutinin
368 (WGA) revealed O-GlcNAc modification of many different proteins, among them a number of
369 transcriptional regulators, including SPLs [40]. SPL9 and SPL15 directly interact with RGA
370 [11, 12, 32], and this interaction is likely to be affected by glycosylation of RGA as it was shown
371 for other transcription factors such as BRASSINAZOLE-RESISTANT 1(BZR1), JASMONATE-
372 ZIM-DOMAIN PROTEIN 1 (JAZ1), PHYTOCHROME INTERACTING FACTOR 3 and 4 (PIF3,
373 PIF4) [38, 39]. Here, we show that SPL15 additionally directly interacts with and is modified
374 by SPY, suggesting that there is an additional, potentially independent effect of glycosylation
375 on SPL15 function. Moreover, we see an additive effect in *spy spl9/15* on leaf size as well as
376 pavement cell size, indicating that SPLs might additionally be regulated by other factors in the
377 determination of leaf size.

Our data indicate that the activity of SPLs is stabilized in both O-glycosylation mutants despite overexpression of *miR156a*, as the late flowering phenotype of *35S::miR156a* is almost completely suppressed in *spy-22 35S::miR156a* and *sec-5 35S::miR156a*. This is supported by the genetic analysis using *spl9/15* crosses with *spy-22* and *sec-5*, where the early flowering of *spy-22* and *sec-5* is partly suppressed, suggesting that functional SPLs are necessary for the accelerated flowering time in O-glycosylation mutants. It has previously been shown that miR156 overexpression lines are less sensitive to GA treatment in terms of flowering time, keeping their extreme late flowering phenotype even when sprayed with GA [9, 11]. *spy*-mutants are often described as showing constitutive gibberellin signalling, but in contrast to gibberellin treatment of miR156 overexpression lines, we see a strong suppression of late flowering in *spy-22 35S::MIR156a* mutants. Moreover, albeit SPY and SEC have opposite effects in gibberellin signalling [38, 39], *sec-5* as well as *spy-22* suppress the late flowering of *35S::MIR156a*, and to a lesser extent developmental transitions, suggesting that the effect of glycosylation on SPLs might be independent of GA signalling and DELLAs, as well as miR156, with a degree of redundancy between O-GlcNAc and O-fucose.

Phenotyping of leaf and rosette growth as well as cellular analysis of our lines suggest a role for both SPY and SPL9/SPL15 in leaf and cell size, with a clear additive effect. Again, we observed a potentially redundant function for SPY and SEC in this respect, although the phenotypes of *sec-5* were very subtle, and not statistically significant. While we did not see an effect of SPY on cell division, we observed a strong positive effect on cell division in *SPL9::rSPL9:GFP.* On the other hand, total cell number was not significantly decreased in *spl9/15*. This may be due to redundancy and potentially higher order *spl* mutants might show a defect in cell division. However, the results of the leaf and rosette growth analysis might reflect different plastochron length or rates of growth and/or development rather than organ size regulation in the analyzed lines. Sampling of leaves at a later timepoint, when the leaves of all lines are fully developed and have reached maturity, might reveal additional cellular effects in these mutants and lead to additional conclusions. It will be interesting to see in further studies, if (1) SPY indeed regulates cell expansion, but not cell division, via SPLs, or if (2) the differences we see in leaf size are a result of different developmental timing and leaf growth rates in *spy-22* and *spl9/15* mutants, or (3) if the effect of SPY on cell expansion is completely independent of SPLs, for instance by interaction with other targets.

Overall, we suggest a model, where O-glycosylation regulates developmental transitions on multiple levels (Figure 7C). In long photoperiods, SPY suppresses expression of *FT*, via interaction with GI [44]. Additionally, glycosylation of RGA regulates its interaction with transcription factors regulating flowering time, such as PIFs [35, 39, 65] and potentially also SPLs [11, 12, 32]. Our data add an additional level of regulation by direct glycosylation of SPLs, controlling them independently of miR156, and potentially also independently of gibberellins.

MATERIAL AND METHODS

Plant Material and growth conditions

Arabidopsis thaliana ecotype Col-0 of was used as wild type. Lines *spy-22* (SALK_090582), *sec-5* (SALK_034290), *spl9-4 spl15-1* (N67865, [14]), *ft-10* (GK-290E08, [66]), FRI SF-2 (N6209) and pSPL9::GFP-rSPL9 (N9954, [9]), all in Col-0 background, were obtained from the European Arabidopsis Stock Centre (NASC) (Scholl et al., 2000). Seeds were surface sterilized with 70% ethanol and transferred ½ Murashige and Skoog medium (2.15 g/L MS

426 Salts, 0.25 g/L MES, pH 5.7, 1% agar). Seeds were stratified in the dark at 4°C for 48 hours.
427 Based upon the experiment the seedlings were germinated and grown in either long day (LD,
428 16 hours light / 8 hours dark) or short day (SD, 8 hours light / 16 hours dark) conditions at
429 22°C. For studying phase change and flowering time, seedlings were transferred to soil at 5
430 days after germination. For all phenotyping experiments, transgenic lines and their wild-type
431 controls were sown in pots filled with soil. After sowing, the seeds were stratified for 3 days at
432 4°C and grown at 21°C under a 16 h day/8 h night regime for 25 days. Experiments were
433 performed with transgenic and wild type seeds harvested from plants that were grown in
434 parallel.
435
436 Flowering time and phase transition quantification
437 Flowering time was quantified by counting the total number of rosette leaves (TRL) produced.
438 Phase transitions were studied by observing the appearance of abaxial trichomes at the lower
439 side of rosette leaves. Rosette leaves without any abaxial trichomes were grouped as juvenile
440 leaves (JL) and rosette leaves with abaxial trichomes were considered adult. Arabidopsis
441 rosettes were harvested and individual leaves were taped to white paper and scanned for
442 representations. Scanned pictures were edited to black and white using Paint 3D.
443
444 RNA extraction and qPCR
445 For expression analysis, seedlings were grown on ½ MS plates. For studying the primary
446 miRNA expression in response to sucrose treatment, sterilized seeds were germinated in 50
447 ml ½ MS liquid media with shaking at 140 rpm. At 5 DAG, seedlings were transferred to ½ MS
448 media supplemented with and without 50 mM sucrose, and seedlings were harvested after 24
449 h. 200 mg of total plant material was used for total RNA extraction using SV Total Isolation
450 System (Promega). 1µg of RNA was used for cDNA synthesis with the iScript™ cDNA
451 Synthesis kit (Bio-Rad). GoTaq® qPCR Master Mix (Promega) was used for quantitative real-
452 time PCR, primers are listed in Table 5 and data was analyzed with Bio-Rad CFX Manager
453 and Microsoft Excel for relative quantification using the 2(-ΔΔC(T))-method [67]. For technical
454 repeats, every sample was done in triplicates, representative results from one of at least two
455 biological replicates are shown (as given in the figure legends). For studying mature miRNA
456 expression, rosette leaves were harvested at the point when Col-0 plants were flowering.
457 Harvested rosette leaves were separated into juvenile and adult leaves, ground in liquid
458 nitrogen and total RNA from approximately 150 mg of ground leaf material was extracted with
459 a ReliaPrep miRNA Cell and Tissue Miniprep System kit (Promega). A stem loop pulsed RT-
460 PCR protocol [8, 68] was used to study the expression of mature miRNA using a Thermo
461 Scientific RevertAid First Strand cDNA synthesis kit and stem-loop primers for miR156 and
462 miR172 listed in Table 5, small nuclear RNA snoR101 was used as internal reference. Equal
463 amounts of each RNA and 1 µM stem loop primer were incubated at 65°C for 5 minutes with
464 10mM dNTPs. RiboLock RNase Inhibitor and a 5X reaction buffer were added and
465 amplification was done for 60 cycles with 30 s of 30°C, 30 s of 42°C and 50°C for 1 s
466 respectively. PCR products were diluted 4x in nuclease free water, qPCR was done with the
467 GoTaq® qPCR Master Mix (Promega). For technical repeats, every sample was done in
468 triplicates. Following qPCR, the data was analysed with Bio-Rad CFX Manager and Microsoft
469 Excel. Representative results from one of three biological replicates are shown.
470
471 Plasmid construction and generation of transgenic lines
472 *miR156a* overexpressing and *SPY::SPY:FLAG* constructs were generated by amplifying the
473 genomic DNA from Col-0, and for transient overexpression, *SPY*, *SPL8* and *SPL15* were

474 amplified from cDNA to generate the respective tagged constructs using Q5 high fidelity DNA
475 polymerase (NEB). The primers (listed in Table 5) contained 5'-overhangs binding to the
476 linearized, NcoI / XhoI-digested backbone of the cloning vector pENTR™ 4. PCR products
477 were excised and purified from agarose gel using GeneJET Gel Extraction Kit (Thermo Fisher)
478 and cloned into Gateway™ pENTR™ 4 by mixing the linearized vector backbone and PCR
479 product in a 1:1 ratio using Gibson assembly (NEB), before transformation into DH10B electro-
480 competent *E. coli* cells. Plasmids containing the gene of interest were extracted using
481 GeneJET Plasmid Miniprep Kit (Thermo Fisher) and confirmed by sequencing.
482 Plant expression vectors were generated using the above created entry clones and destination
483 vectors pK7WG2D (Karimi et al., 2002) for *35S::MIR156a*, pEarleyGate202 for
484 *35S::FLAG:SPY*, pEarleyGate201 for *35S::HA:SPL8* or *35S::HA:SPL15* and pEarleyGate302
485 for *SPY::SPY:FLAG* (Earley et al., 2006). Recombination of the entry clones with the
486 destination vectors was done using Gateway LR Clonase II enzyme mix. Positive colonies with
487 the plasmid of interest were selected for spectinomycin (150µg/mL) resistance for miRNA
488 overexpressing pK7WG2D constructs, and kanamycin (50µg/mL) resistance for
489 pEarleyGate201, pEarleyGate202 and pEarleyGate302 constructs, respectively on LB
490 medium. Plasmids carrying the gene of interest were extracted from overnight bacterial culture
491 using GeneJET Plasmid Miniprep Kit (Thermo Fisher) and confirmed by sequencing. Correct
492 plasmids were transformed to *Agrobacterium tumefaciens* strain GV3101 (pMP90) before
493 transformation of plants by floral dipping [69]. *35S:MIR156a* constructs were transformed to
494 Col-0, then crossed to *spy-22* and *sec-5* backgrounds, and *SPY::SPY:FLAG* was introduced
495 into *spy-22* background.
496
497 Rosette growth and leaf series analysis
498 For the projected rosette measurements over time, pots containing the plants were positioned
499 in a randomized way for 25 DAS on a platform, named MIRGIS, allowing fully automatic
500 phenotyping. Pictures were acquired on a daily interval and image processing and analysis
501 were performed using the ImageJ software (http://rsb.info.nih.gov/ij/). To construct the
502 projected rosette area and rosette growth curves, the area measurements of similar transgenic
503 lines plants were compiled. For the leaf series analysis, individual leaves (cotyledons and
504 rosette leaves) of 25 day-old plants were dissected at the base of the petiole, oriented from
505 old (cotyledons) to young on a thin layer of 1% w/v agar covering the bottom of a square plate
506 (22.5 x 22.5 cm) and, if necessary, cut to flatten them. The leaf series were imaged and the
507 individual leaf areas were measured with the ImageJ software (http://rsb.info.nih.gov/ij/). The
508 real rosette area was defined as the sum of the individual plant leaves. The growth experiment
509 was performed in three independent biological repeats containing 8 plants per experiment.
510
511 Cellular analysis
512 Following the leaf series analysis at 25 DAS, the first leaf pairs (L1/2; 16 leaves) were cleared
513 with 100% ethanol, stored in lactic acid and mounted on microscopic slides. The leaves were
514 photographed with a dark-field binocular microscope and the leaf blade areas were
515 determined with the ImageJ software. For each line, three leaves with an area closest to the
516 median and the average were selected for detailed cellular analysis. Abaxial (lower) epidermal
517 cells (~150 cells) at the tip of the leaves were drawn with a binocular microscope (Leica,
518 DMLB) fitted with a drawing tube and a differential interference contrast objective. The
519 microscopic drawings were scanned for digitalization and guard, pavement and total cell
520 numbers, as well as pavement cell area, stomatal density, stomatal index were calculated with

521 the ImageJ software, as described in [19]. The cellular analysis experiment was performed in
522 three independent biological repeats.
523
524 Transient protein expression in *N. benthamiana*
525 For transient expression in *N. benthamiana*, *Agrobacterium tumefaciens* strain, GV3101
526 (pMP90) expressing *35S::FLAG:SPY* and *35S::HA:SPL8* or *-SPL15* constructs were
527 cultivated overnight using rifampicin (50µg/mL), gentamycin (50µg/mL) and kanamycin
528 (50µg/mL) selection. Bacterial cells were harvested, washed and resuspended in infiltration
529 medium (500 mM MES, 20 mM Na_3PO_4, 100 µM acetosyringone, 50 mg/L D-glucose) to
530 OD600 of 0.5. For co-infiltration, equal amounts of the respective cultures were mixed. After
531 infiltration on the abaxial side of a leaf of a five-week old *N. benthamiana* plant, the plants
532 were maintained in the growth chamber for 3 days before harvesting.
533
534 Protein extraction and co-immunoprecipitation
535 For protein extraction, 1 g of agro-infiltrated leaves were frozen in liquid nitrogen, ground and
536 taken up in 50 mM Tris-HCl pH 7.6, 150 mM NaCl, 1% Triton X-100, 1x plant protease inhibitor
537 cocktail (Sigma) and 20 µM PUGNAc in the ratio 2:1. 100µL extract was stored for further
538 analysis as input. 50 µL of anti-FLAG beads (Miltenyi Biotec) were added to the remaining
539 plant extract and the samples were incubated on a rotor at 4°C for 30 minutes. A µMACS
540 column was placed in the magnetic field of a µMACS separator and washed with above
541 mentioned 200 µL extraction buffer. Plant extract containing the anti-FLAG beads was added
542 to the column and 100 µL of the flow-through were collected and saved for further analysis.
543 The column was rinsed 4 times with 200 µL TBS (50 mM Tris-HCl pH 7.5, 150 mM NaCl, 1x
544 plant protease inhibitor cocktail (Sigma), 20 µM PuGNAc, 1.5 mM DTE) and once with 100 µL
545 wash buffer (20 mM Tris-HCl pH 7.5). For elution, 20µL 0.1 M glycine, pH 2.3 was loaded onto
546 to the column and incubated for 3-5 minutes. After adding 60µL 0.1 M glycine the first eluate
547 was collected and neutralized with 20 µL 0.5 M Tris, pH 8.0. In the next step 20 µL of pre-
548 heated 95°C hot Laemmli buffer (10% glycerol, 60 mM Tris-HCl pH 6.8, 2% SDS, 0.1%
549 bromophenol blue, 5% β-mercaptoethanol) was loaded to the column and incubated for 5
550 minutes. Subsequently, 80 µL of pre-heated 95°C hot Laemmli buffer were added and the
551 eluate was collected and used for SDS-PAGE analysis and Western blotting.
552
553 Western Blotting and antibody dilutions
554 Input samples and eluates from the co-immunoprecipitation from both individual and co-
555 infiltrated samples were subjected to SDS PAGE, and transferred to a PVDF membrane (Roth
556 Roti®-PVDF, pore size 0.45 µm) using the wet transfer method in the Mini-Protean Tetra-
557 System (Bio-Rad). The membranes were washed with PBST (137 mM NaCl, 2.7 mM KCl, 10
558 mM Na_2HPO_4, 1.8 mM KH_2PO_4, 0.1% (v/v) Tween 80) for 10 minutes, blocked with 3% milk
559 for 1 hour at room temperature and probed with anti-FLAG M2 monoclonal antibody (mouse,
560 Sigma F1804, 1:2000 in 3% milk/PBST), or blocked with 5% BSA for 1 hour at room
561 temperature and probed with anti-HA antibody (rabbit, Cell Signaling Technology 3742S,
562 1:1000 in 5% BSA/PBST) respectively. After probing at 4°C overnight, the membranes were
563 washed with PBST before incubation with the respective secondary antibodies, goat anti-
564 mouse HRP (1:10000) (Dianova 115-035-164), and goat anti-rabbit HRP (1:20000, Agrisera
565 A S09 602) for 1 hour at room temperature. After washing, Bio-Rad Clarity Western ECL
566 substrate was used for chemiluminescence detection on a Fusion Solo S (Vilber).
567
568 Data and statistical analysis

569 We used Excel for analysis of gene expression, and GraphPad Prism 5 and R (*ggplot2*, R
570 Core Team, https://www.r-project.org/) for statistical analysis and generating graphs for
571 quantification of rosette leaves. In the leaf quantification graphs, the mean is shown and error
572 bars represent standard error, n is given in the respective tables. For statistical analysis, one-
573 way ANOVA followed by Tukey's multiple comparison test were done. For the leaf series
574 analysis, statistical tests were performed with the mixed models and plm procedure using SAS
575 Enterprise Guide 7 software as described previously in [70]. An F-test ($p<0.05$) was used to
576 assess equality of variances. For each leaf, pairwise comparisons amongst the transgenic line
577 or between the transgenic lines and the wild type control were performed using a Tukey-
578 Kramer post-hoc analysis ($p < 0.05$). For the statistical analysis of the leaf blade area of L1/2
579 and the cellular data, ANOVA tests were performed in R (version 3.3.2) (https://www.r-
580 project.org) followed by Tukey's multiple comparison test ($p < 0.05$). For all statistical tests,
581 the transgenic line was included as the fixed factor in the model. All experiments were
582 performed in three biological replicates and the repeat factor was included as a random factor.
583

584 **ACKNOWLEDGEMENTS**

585 We gratefully acknowledge Marie-Theres Hauser for sharing equipment, Lukas Grinninger for
586 technical support and Julia König for supplying *N. benthamiana* plants. We thank Barbara
587 Korbei, Vinod Kumar and Jürgen Kleine-Vehn for valuable input. This work was supported by
588 the Austrian Academy of Sciences ÖAW (DOC-fellowship to K.V.M. and APART fellowship to
589 D.L.) and the Austrian Science Fund FWF (P-29051). A.B. received funding from the Research
590 Foundation Flanders (FWO) under the project number 3G038719.
591

592 **AUTHOR CONTRIBUTIONS:**

593 D.L. conceived the project, D.L., K.V.M designed experiments and wrote the manuscript. A.B.
594 designed and performed phenotyping and cellular analysis, K.V.M. performed all other
595 experiments with the help of N.N., C.F. and I.Z.
596

597 **DECLARATION OF INTERESTS**

598 The authors declare no competing interests.
599

600 **REFERENCES**

601

602 1. Poethig, R.S. (2003). Phase change and the regulation of developmental timing in
603 plants. Science *301*, 334-336.
604 2. Baurle, I., and Dean, C. (2006). The timing of developmental transitions in plants. Cell
605 *125*, 655-664.
606 3. Huijser, P., and Schmid, M. (2011). The control of developmental phase transitions in
607 plants. Development *138*, 4117-4129.
608 4. He, J., Xu, M., Willmann, M.R., McCormick, K., Hu, T., Yang, L., Starker, C.G., Voytas,
609 D.F., Meyers, B.C., and Poethig, R.S. (2018). Threshold-dependent repression of SPL
610 gene expression by miR156/miR157 controls vegetative phase change in Arabidopsis
611 thaliana. PLoS genetics *14*, e1007337.
612 5. Fouracre, J.P., and Poethig, R.S. (2016). The role of small RNAs in vegetative shoot
613 development. Current opinion in plant biology *29*, 64-72.
614 6. Poethig, R.S. (2009). Small RNAs and developmental timing in plants. Curr Opin
615 Genet Dev *19*, 374-378.

616 7. Wu, G., Park, M.Y., Conway, S.R., Wang, J.W., Weigel, D., and Poethig, R.S. (2009).
617 The sequential action of miR156 and miR172 regulates developmental timing in
618 Arabidopsis. Cell *138*, 750-759.
619 8. Xu, M., Hu, T., Zhao, J., Park, M.Y., Earley, K.W., Wu, G., Yang, L., and Poethig, R.S.
620 (2016). Developmental Functions of miR156-Regulated SQUAMOSA PROMOTER
621 BINDING PROTEIN-LIKE (SPL) Genes in Arabidopsis thaliana. PLoS genetics *12*,
622 e1006263.
623 9. Wang, J.W., Czech, B., and Weigel, D. (2009). miR156-regulated SPL transcription
624 factors define an endogenous flowering pathway in Arabidopsis thaliana. Cell *138*,
625 738-749.
626 10. Yang, L., Conway, S.R., and Poethig, R.S. (2011). Vegetative phase change is mediated
627 by a leaf-derived signal that represses the transcription of miR156. Development
628 *138*, 245-249.
629 11. Yu, S., Galvao, V.C., Zhang, Y.C., Horrer, D., Zhang, T.Q., Hao, Y.H., Feng, Y.Q., Wang,
630 S., Schmid, M., and Wang, J.W. (2012). Gibberellin regulates the Arabidopsis floral
631 transition through miR156-targeted SQUAMOSA promoter binding-like transcription
632 factors. The Plant cell *24*, 3320-3332.
633 12. Hyun, Y., Richter, R., Vincent, C., Martinez-Gallegos, R., Porri, A., and Coupland, G.
634 (2016). Multi-layered Regulation of SPL15 and Cooperation with SOC1 Integrate
635 Endogenous Flowering Pathways at the Arabidopsis Shoot Meristem. Dev Cell *37*,
636 254-266.
637 13. Jung, J.H., Ju, Y., Seo, P.J., Lee, J.H., and Park, C.M. (2012). The SOC1-SPL module
638 integrates photoperiod and gibberellic acid signals to control flowering time in
639 Arabidopsis. The Plant journal : for cell and molecular biology *69*, 577-588.
640 14. Schwarz, S., Grande, A.V., Bujdoso, N., Saedler, H., and Huijser, P. (2008). The
641 microRNA regulated SBP-box genes SPL9 and SPL15 control shoot maturation in
642 Arabidopsis. Plant Mol Biol *67*, 183-195.
643 15. Xing, S., Salinas, M., Höhmann, S., Berndtgen, R., and Huijser, P. (2010). miR156-
644 Targeted and Nontargeted SBP-Box Transcription Factors Act in Concert to Secure
645 Male Fertility in Arabidopsis. The Plant Cell *22*, 3935-3950.
646 16. Yang, L., Xu, M., Koo, Y., He, J., and Poethig, R.S. (2013). Sugar promotes vegetative
647 phase change in Arabidopsis thaliana by repressing the expression of MIR156A and
648 MIR156C. Elife *2*, e00260.
649 17. Yu, S., Cao, L., Zhou, C.M., Zhang, T.Q., Lian, H., Sun, Y., Wu, J., Huang, J., Wang, G.,
650 and Wang, J.W. (2013). Sugar is an endogenous cue for juvenile-to-adult phase
651 transition in plants. eLife *2*, e00269.
652 18. Czesnick, H., and Lenhard, M. (2015). Size control in plants--lessons from leaves and
653 flowers. Cold Spring Harb Perspect Biol *7*, a019190.
654 19. Andriankaja, M., Dhondt, S., De Bodt, S., Vanhaeren, H., Coppens, F., De Milde, L.,
655 Muhlenbock, P., Skirycz, A., Gonzalez, N., Beemster, G.T., et al. (2012). Exit from
656 proliferation during leaf development in Arabidopsis thaliana: a not-so-gradual
657 process. Dev Cell *22*, 64-78.
658 20. Debernardi, J.M., Mecchia, M.A., Vercruyssen, L., Smaczniak, C., Kaufmann, K., Inze,
659 D., Rodriguez, R.E., and Palatnik, J.F. (2014). Post-transcriptional control of GRF
660 transcription factors by microRNA miR396 and GIF co-activator affects leaf size and
661 longevity. The Plant journal : for cell and molecular biology *79*, 413-426.

662 21. Jaeger, K.E., and Wigge, P.A. (2007). FT protein acts as a long-range signal in
663 Arabidopsis. Current biology : CB *17*, 1050-1054.
664 22. Wigge, P.A., Kim, M.C., Jaeger, K.E., Busch, W., Schmid, M., Lohmann, J.U., and
665 Weigel, D. (2005). Integration of spatial and temporal information during floral
666 induction in Arabidopsis. Science *309*, 1056-1059.
667 23. Mathieu, J., Warthmann, N., Kuttner, F., and Schmid, M. (2007). Export of FT protein
668 from phloem companion cells is sufficient for floral induction in Arabidopsis. Current
669 biology : CB *17*, 1055-1060.
670 24. Andres, F., and Coupland, G. (2012). The genetic basis of flowering responses to
671 seasonal cues. Nat Rev Genet *13*, 627-639.
672 25. Wittwer, S.H., and Bukovac, M.J. (1957). Gibberellin Effects on Temperature and
673 Photoperiodic Requirements for Flowering of Some Plants. Science *126*, 30-31.
674 26. Brian, P.W. (1958). Role of gibberellin-like hormones in regulation of plant growth &
675 flowering. Nature *181*, 1122-1123.
676 27. Wilson, R.N., Heckman, J.W., and Somerville, C.R. (1992). Gibberellin Is Required for
677 Flowering in Arabidopsis thaliana under Short Days. Plant Physiol *100*, 403-408.
678 28. Reeves, P.H., and Coupland, G. (2001). Analysis of flowering time control in
679 Arabidopsis by comparison of double and triple mutants. Plant Physiol *126*, 1085-
680 1091.
681 29. Moon, J., Suh, S.S., Lee, H., Choi, K.R., Hong, C.B., Paek, N.C., Kim, S.G., and Lee, I.
682 (2003). The SOC1 MADS-box gene integrates vernalization and gibberellin signals for
683 flowering in Arabidopsis. The Plant journal : for cell and molecular biology *35*, 613-
684 623.
685 30. Achard, P., Herr, A., Baulcombe, D.C., and Harberd, N.P. (2004). Modulation of floral
686 development by a gibberellin-regulated microRNA. Development *131*, 3357-3365.
687 31. Porri, A., Torti, S., Romera-Branchat, M., and Coupland, G. (2012). Spatially distinct
688 regulatory roles for gibberellins in the promotion of flowering of Arabidopsis under
689 long photoperiods. Development *139*, 2198-2209.
690 32. Yamaguchi, N., Winter, C.M., Wu, M.F., Kanno, Y., Yamaguchi, A., Seo, M., and
691 Wagner, D. (2014). Gibberellin acts positively then negatively to control onset of
692 flower formation in Arabidopsis. Science *344*, 638-641.
693 33. Galvao, V.C., Collani, S., Horrer, D., and Schmid, M. (2015). Gibberellic acid signaling
694 is required for ambient temperature-mediated induction of flowering in Arabidopsis
695 thaliana. The Plant journal : for cell and molecular biology *84*, 949-962.
696 34. Harberd, N.P., Belfield, E., and Yasumura, Y. (2009). The angiosperm gibberellin-
697 GID1-DELLA growth regulatory mechanism: how an "inhibitor of an inhibitor"
698 enables flexible response to fluctuating environments. The Plant cell *21*, 1328-1339.
699 35. de Lucas, M., Daviere, J.M., Rodriguez-Falcon, M., Pontin, M., Iglesias-Pedraz, J.M.,
700 Lorrain, S., Fankhauser, C., Blazquez, M.A., Titarenko, E., and Prat, S. (2008). A
701 molecular framework for light and gibberellin control of cell elongation. Nature *451*,
702 480-484.
703 36. Feng, S., Martinez, C., Gusmaroli, G., Wang, Y., Zhou, J., Wang, F., Chen, L., Yu, L.,
704 Iglesias-Pedraz, J.M., Kircher, S., et al. (2008). Coordinated regulation of Arabidopsis
705 thaliana development by light and gibberellins. Nature *451*, 475-479.
706 37. Li, Q.F., Wang, C., Jiang, L., Li, S., Sun, S.S., and He, J.X. (2012). An interaction
707 between BZR1 and DELLAs mediates direct signaling crosstalk between
708 brassinosteroids and gibberellins in Arabidopsis. Science signaling *5*, ra72.

38. Zentella, R., Hu, J., Hsieh, W.P., Matsumoto, P.A., Dawdy, A., Barnhill, B., Oldenhof, H., Hartweck, L.M., Maitra, S., Thomas, S.G., et al. (2016). O-GlcNAcylation of master growth repressor DELLA by SECRET AGENT modulates multiple signaling pathways in Arabidopsis. Genes Dev *30*, 164-176.
39. Zentella, R., Sui, N., Barnhill, B., Hsieh, W.P., Hu, J., Shabanowitz, J., Boyce, M., Olszewski, N.E., Zhou, P., Hunt, D.F., et al. (2017). The Arabidopsis O-fucosyltransferase SPINDLY activates nuclear growth repressor DELLA. Nature chemical biology.
40. Xu, S.L., Chalkley, R.J., Maynard, J.C., Wang, W., Ni, W., Jiang, X., Shin, K., Cheng, L., Savage, D., Huhmer, A.F., et al. (2017). Proteomic analysis reveals O-GlcNAc modification on proteins with key regulatory functions in Arabidopsis. Proceedings of the National Academy of Sciences of the United States of America *114*, E1536-E1543.
41. Silverstone, A.L., Tseng, T.-S., Swain, S.M., Dill, A., Jeong, S.Y., Olszewski, N.E., and Sun, T.-p. (2007). Functional Analysis of SPINDLY in Gibberellin Signaling in Arabidopsis. Plant Physiology *143*, 987-1000.
42. Swain, S.M., Tseng, T.-s., and Olszewski, N.E. (2001). Altered Expression of SPINDLY Affects Gibberellin Response and Plant Development. Plant Physiology *126*, 1174-1185.
43. Tseng, T.-S., Swain, S.M., and Olszewski, N.E. (2001). Ectopic Expression of the Tetratricopeptide Repeat Domain of SPINDLY Causes Defects in Gibberellin Response. Plant Physiology *126*, 1250-1258.
44. Tseng, T.-S., Salomé, P.A., McClung, C.R., and Olszewski, N.E. (2004). SPINDLY and GIGANTEA Interact and Act in Arabidopsis thaliana Pathways Involved in Light Responses, Flowering, and Rhythms in Cotyledon Movements. The Plant Cell Online *16*, 1550-1563.
45. Xing, L., Liu, Y., Xu, S., Xiao, J., Wang, B., Deng, H., Lu, Z., Xu, Y., and Chong, K. (2018). Arabidopsis O-GlcNAc transferase SEC activates histone methyltransferase ATX1 to regulate flowering. EMBO J *37*.
46. Clarke, J.H., and Dean, C. (1994). Mapping FRI, a locus controlling flowering time and vernalization response in Arabidopsis thaliana. Molecular & general genetics : MGG *242*, 81-89.
47. Lee, I., and Amasino, R.M. (1995). Effect of Vernalization, Photoperiod, and Light Quality on the Flowering Phenotype of Arabidopsis Plants Containing the FRIGIDA Gene. Plant Physiol *108*, 157-162.
48. Yu, S., Lian, H., and Wang, J.W. (2015). Plant developmental transitions: the role of microRNAs and sugars. Curr Opin Plant Biol *27*, 1-7.
49. Telfer, A., Bollman, K.M., and Poethig, R.S. (1997). Phase change and the regulation of trichome distribution in Arabidopsis thaliana. Development *124*, 645-654.
50. Willmann, M.R., and Poethig, R.S. (2011). The effect of the floral repressor FLC on the timing and progression of vegetative phase change in Arabidopsis. Development *138*, 677-685.
51. Wu, G., and Poethig, R.S. (2006). Temporal regulation of shoot development in Arabidopsis thaliana by miR156 and its target SPL3. Development *133*, 3539-3547.
52. Olivier-Van Stichelen, S., Dehennaut, V., Buzy, A., Zachayus, J.-L., Guinez, C., Mir, A.-M., El Yazidi-Belkoura, I., Copin, M.-C., Boureme, D., Loyaux, D., et al. (2014). O-GlcNAcylation stabilizes β-catenin through direct competition with phosphorylation at threonine 41. The FASEB Journal *28*, 3325-3338.

53. Walgren, J.L., Vincent, T.S., Schey, K.L., and Buse, M.G. (2003). High glucose and insulin promote O-GlcNAc modification of proteins, including alpha-tubulin. American journal of physiology. Endocrinology and metabolism *284*, E424-434.
54. Peng, C., Zhu, Y., Zhang, W., Liao, Q., Chen, Y., Zhao, X., Guo, Q., Shen, P., Zhen, B., Qian, X., et al. (2017). Regulation of the Hippo-YAP Pathway by Glucose Sensor O-GlcNAcylation. Mol Cell *68*, 591-604 e595.
55. Hart, G.W. (2014). Nutrient Regulation of Cellular Metabolism & Physiology by O-GlcNAcylation. Journal of Biological Chemistry.
56. Wang, J.W., Schwab, R., Czech, B., Mica, E., and Weigel, D. (2008). Dual effects of miR156-targeted SPL genes and CYP78A5/KLUH on plastochron length and organ size in Arabidopsis thaliana. Plant Cell *20*, 1231-1243.
57. Strasser, R. (2016). Plant protein glycosylation. Glycobiology *26*, 926-939.
58. Halim, A., Larsen, I.S., Neubert, P., Joshi, H.J., Petersen, B.L., Vakhrushev, S.Y., Strahl, S., and Clausen, H. (2015). Discovery of a nucleocytoplasmic O-mannose glycoproteome in yeast. Proceedings of the National Academy of Sciences of the United States of America *112*, 15648-15653.
59. Bandini, G., Haserick, J.R., Motari, E., Ouologuem, D.T., Lourido, S., Roos, D.S., Costello, C.E., Robbins, P.W., and Samuelson, J. (2016). O-fucosylated glycoproteins form assemblies in close proximity to the nuclear pore complexes of Toxoplasma gondii. Proceedings of the National Academy of Sciences of the United States of America *113*, 11567-11572.
60. Steiner, E., Efroni, I., Gopalraj, M., Saathoff, K., Tseng, T.S., Kieffer, M., Eshed, Y., Olszewski, N., and Weiss, D. (2012). The Arabidopsis O-linked N-acetylglucosamine transferase SPINDLY interacts with class I TCPs to facilitate cytokinin responses in leaves and flowers. The Plant cell *24*, 96-108.
61. Steiner, E., Livne, S., Kobinson-Katz, T., Tal, L., Pri-Tal, O., Mosquna, A., Tarkowska, D., Mueller, B., Tarkowski, P., and Weiss, D. (2016). The Putative O-Linked N-Acetylglucosamine Transferase SPINDLY Inhibits Class I TCP Proteolysis to Promote Sensitivity to Cytokinin. Plant physiology *171*, 1485-1494.
62. Cui, H., Kong, D., Wei, P., Hao, Y., Torii, K.U., Lee, J.S., and Li, J. (2014). SPINDLY, ERECTA, and Its Ligand STOMAGEN Have a Role in Redox-Mediated Cortex Proliferation in the Arabidopsis Root. Molecular plant.
63. Sarnowska, E.A., Rolicka, A.T., Bucior, E., Cwiek, P., Tohge, T., Fernie, A.R., Jikumaru, Y., Kamiya, Y., Franzen, R., Schmelzer, E., et al. (2013). DELLA-interacting SWI3C core subunit of switch/sucrose nonfermenting chromatin remodeling complex modulates gibberellin responses and hormonal cross talk in Arabidopsis. Plant Physiol *163*, 305-317.
64. Hartweck, L.M., Genger, R.K., Grey, W.M., and Olszewski, N.E. (2006). SECRET AGENT and SPINDLY have overlapping roles in the development of Arabidopsis thaliana L. Heyn. Journal of Experimental Botany *57*, 865-875.
65. Kumar, S.V., Lucyshyn, D., Jaeger, K.E., Alos, E., Alvey, E., Harberd, N.P., and Wigge, P.A. (2012). Transcription factor PIF4 controls the thermosensory activation of flowering. Nature *484*, 242-245.
66. Yoo, S.K., Chung, K.S., Kim, J., Lee, J.H., Hong, S.M., Yoo, S.J., Yoo, S.Y., Lee, J.S., and Ahn, J.H. (2005). CONSTANS activates SUPPRESSOR OF OVEREXPRESSION OF CONSTANS 1 through FLOWERING LOCUS T to promote flowering in Arabidopsis. Plant Physiol *139*, 770-778.

803 67. Livak, K.J., and Schmittgen, T.D. (2001). Analysis of relative gene expression data
804 using real-time quantitative PCR and the 2(-Delta Delta C(T)) Method. Methods (San
805 Diego, Calif.) *25*, 402-408.
806 68. Varkonyi-Gasic, E., Wu, R., Wood, M., Walton, E.F., and Hellens, R.P. (2007).
807 Protocol: a highly sensitive RT-PCR method for detection and quantification of
808 microRNAs. Plant Methods *3*, 12.
809 69. Clough, S.J., and Bent, A.F. (1998). Floral dip: a simplified method for Agrobacterium-
810 mediated transformation of Arabidopsis thaliana. The Plant journal : for cell and
811 molecular biology *16*, 735-743.
812 70. Blomme, J., Inze, D., and Gonzalez, N. (2014). The cell-cycle interactome: a source of
813 growth regulators? J Exp Bot *65*, 2715-2730.
814
815

816 **TABLES**
817
818 **Table 1:Rosette leaf numbers for graphs shown in Figure 1**
819

		Rosette leaves (average ± SD)	n
LD	Col-0	13.1 ± 1.1	51
	spy-22 [a]	8.6 ± 1.4	46
	sec-5 [a]	11.8 ± 1.6	49
SD	Col-0	61.0 ± 6.1	33
	spy-22	20.7 ± 3.1	33
	sec-5	60.5 ± 6.7	30
LD		**Rosette leaves (average ± SD)**	**n**
	Col-0	14.6 ± 1.3	13
	ft-10	47.6 ± 2.9	9
	spy-22	7.1 ± 0.6	13
	sec-5	14.9 ± 1.5	11
	ft-10 spy-22	17.4 ± 1.3	11
	ft-10 sec -5	46.2 ± 6.4	8
		Rosette leaves (average ± SD)	**n**
	Col-0	14.7 ± 1.3	13
	spy-22	7.1 ± 0.7	13
	FRI	74.2 ± 7.8	12
	FRI *spy-22*	26.0 ± 1.4	10

820
821 average ± SD is given
822 One-way ANOVA, Tukeys Multiple Comparison Test:
823 [a] significantly lower than Col-0 (*** $p \leq 0.001$)
824
825 **Table 2: Rosette leaf numbers for graphs shown in Figure 2**
826

		Juvenile leaves	n	Rosette leaves	n
LD	Col-0	5.8 ± 0.6	42	12.6 ± 1.2	56
	spy-22 [a]	3.5 ± 0.6 ***	33	7.8 ± 1.1 ***	45
	sec-5 [a]	5.9 ± 0.7 ns	31	11.4 ± 1.03***	45
		Juvenile leaves	**n**	**Rosette leaves**	**n**
	Col-0	5.0 ± 0.6	22	14.6 ± 1.3	13
	spy-22	3.6 ± 0.5	19	7.1 ± 0.6	13
	ft-10	9.2 ± 1.0	20	47.6 ± 2.9	9
	ft-10 spy-22	3.5 ± 0.6	16	17.4 ± 1.3	11

827
828 average ± SD is given
829 One-way ANOVA, Tukeys Multiple Comparison Test:
830 [a] significantly lower than Col-0 (*** $p \leq 0.001$)
831 [b] significantly less rosette leaves than Col-0 (* $p \leq 0.05$)
832
833
834 **Table 3: Rosette leaf numbers for graphs shown in Figure 3**
835

	Rosette leaves (average ± SD)	n
Col-0	10 ± 0.9	12
spy-22	8 ± 0.6	10
sec-5	9.8 ± 0.9	11
35S::MIR156a Col-0	51.8 ± 6.8	11
35S::MIR156a spy-22	9 ± 1.2	24
35S::MIR156a sec-5	11.3 ± 1.2	22

836
837 average ± SD is given
838
839
840
841
842

Table 4: Rosette leaf numbers for graphs shown in Figure 4

		Juvenile leaves	n	Rosette leaves	n
LD	Col-0	5.8 ± 0.6	42	12.6 ± 1.2	56
	spy-22 [d]	3.5 ± 0.6	33	7.8 ± 1.1 ***	45
	sec-5 [d]	5.9 ± 0.7 ns	31	11.4 ± 1.03***	45
	spl9-4/15-1 [e]	8.8 ± 0.6	37	19.6 ± 2.2	49
	spy-22 spl9-4/15-1 [a b]	5.4 ± 0.7	42	10.2 ± 1.5	54
	sec-5 spl9-4/15-1 [a c]	6.8 ± 0.7	46	16.3 ± 1.5	60
	SPL9::rSPL9:GFP	1.3 ± 0.5	37	5.4 ± 1.1	50

average ± SD is given
One-way ANOVA, Tukeys Multiple Comparison Test:
[a] significantly more juvenile and rosette leaves than *spy-22* or *sec-5* (*** $p \leq 0.001$),
[b] significantly less juvenile and rosette leaves than *spl9-4/15-1* (*** $p \leq 0.001$)
[c] significantly less juvenile leaves than *spl9-4/15-1* (** $p \leq 0.01$)
[d] significantly less rosette leaves than Col-0 (*** $p \leq 0.001$)
[e] significantly more rosette leaves than Col-0 (*** $p \leq 0.001$)

Table 5: Distribution of pavement cell circularity and area

Distribution of pavement cell area							
Cell area ($x10^3$ µm²)	**Col-0**	***spy-22***	***sec-5***	***spl9/15***	***spy-22 spl9/15***	***sec-5 spl9/15***	***rSPL9***
< 4	26,82	32,73	28,96	28,94	38,77	31,49	23,18
4-8	36,59	45,05	38,03	39,90	48,27	39,94	42,88
8-12	22,74	18,77	21,68	23,97	12,35	20,58	21,36
12-16	10,83	3,15	8,74	4,62	0,62	5,84	6,29
16-20	2,49	0,30	2,43	2,57	0,00	2,15	3,81
20-24	0,53	0,00	0,16	0,00	0,00	0,00	1,66
>24	0,00	0,00	0,00	0,00	0,00	0,00	0,83
Sum (%)	100,00	100,00	100,00	100,00	100,00	100,00	100,00

898 **Table 6: Oligonucleotides used in this study**
899

ID	Sequence	Orientation	Purpose
At5g60390 (EF1α)	TGAGCACGCTCTTCTTGCTTTCA	forward	qPCR, reference
	GGTGGTGGCATCCATCTTGTTACA	reverse	
pri-miR156a	CTTCGTTCTCTATGTCTCAATCTCTC	forward	qPCR [16]
	TGATTAAAGGCTAAAGGTCTCCTC	reverse	
pri-miR156b	GTGATAATGAGTGATGACTGATG	forward	qPCR [16]
	GAAAACGTGACCGGGACCGAATCG	reverse	
pri-miR156c	GTGATAATGAGTGATGACTGATG	forward	qPCR [16]
	GAAAACGTGACCGGGACCGAATCG	reverse	
FT	CATTTTATGATACGAGTAACGAACGGTG	forward	qPCR
	CACTCTCATTTTCCTCCCCCTCTC	reverse	
FLC	TCATGTGGGAGCAGAAGCTG	forward	qPCR
	CCGCCGATTTAAGGTGGCTA	reverse	
miR156	GTCGTATCCAGTGCAGGGTCCGAGGTATTCGCACTGGATACGAC GTGCTCA	stem-loop for RT	qPCR/miRNA-quantification [8]
miR172	GTCGTATCCAGTGCAGGGTCCGAGGTATTCGCACTGGATACGAC ATGCAG	stem-loop for RT	qPCR/miRNA-quantification [8]
snoR101	CTTCACAGGTAAGTTCGCTTG	forward	qPCR/miRNA-quantification [8]
	AGCATCAGCAGACCAGTAGTT	reverse	
miR172	CGGCGGAGAATCTTGATGATGC	forward	qPCR/miRNA-quantification [8]
	GTGCAGGGTCCGAGGT	reverse	
miR156	GCGGCGGTGACAGAAGAGAGT	forward	qPCR/miRNA-quantification [8]
	GTGCAGGGTCCGAGGT	reverse	

900

ID	Sequence	Orientation	Purpose
spy-22	GTTAAACCCTAAGTATCGGAC	forward	Genotyping
	TTGGCATAAGAAAGTGTATC	reverse	
	ATTTTGCCGATTTCGGAAC	T-DNA	
sec-5	CACGCCTGGCTCTTGCTCATCAG	forward	Genotyping
	GCGGATTGCACGATCAGTGTC	reverse	
	ATTTTGCCGATTTCGGAAC	T-DNA	
spl 15-1	TGTTGGTGTCTGAAGTTGCTG	forward	Genotyping
	TCCACCGAGTCTTCTTCACTC	reverse	
	TGGTTCACGTAGTGGGCCATCG	T-DNA	
spl 9-4	TGGTTCCTCCACTGAGTCATC	forward	Genotyping
	GCTCATTATGACCAGCGAGTC	reverse	
	TAGCATCTGAATTTCATAACCAATCTCGATACAC	T-DNA	
ft-10	TAAGCTCAATGATATTCCCGTACA	forward	Genotyping
	CAGGTTCAAAACAAGCCAAGA	T-DNA	
	CCCATTTGGACGTGAATGTAGACAC	reverse	
Col-0 FRI	ATGAGATTGCCGGTGCTTT	forward	Genotyping
	TGGTCGATGATGTCAACAAAA	reverse	

901

ID	Sequence	Orientation	Purpose
miRNA156	TACAAAAAAGCAGGCTCCACTCTTTGTCTTCTCCAGTTAAAAC	forward	Cloning *35::miRNA156a*
	GCTGGGTCTAGATATCTCGACAAGAGAGACAGAGAAAG	reverse	
SPY	TACAAAAAAGCAGGCTCCACAGACAAGAGGGTTTTATAACTC	forward	Cloning SPY-promotor + Flag
	TGTCGTCATCGTCTTTGTAGTCCATTTTTTTGTAACTAAAATCTTG	reverse	
	CTACAAAGACGATGACGACAAGGTGGGACTGGAAGATGATAC	forward	Cloning Flag + SPY-ORF
	GCTGGGTCTAGATATCTCGACTAGCTAGTGGAGTCCATTC	reverse	
SPL8	TACAAAAAAGCAGGCTCCACCTCCTCCACCCCTTCCG	forward	Cloning *35S::HA:SPL8*
	GCTGGGTCTAGATATCTCGATCCGCTGGAGAAAAACATTG	reverse	
SPL15	TACAAAAAAGCAGGCTCCACCACCATGGAGTTGTTAATGTGTTC	forward	Cloning *35S::HA:SPL8*
	GCTGGGTCTAGATATCTCGATCAAAGAGACCAATTGAAATG	reverse	

902

904 **FIGURES**
905
906 Figure 1
907

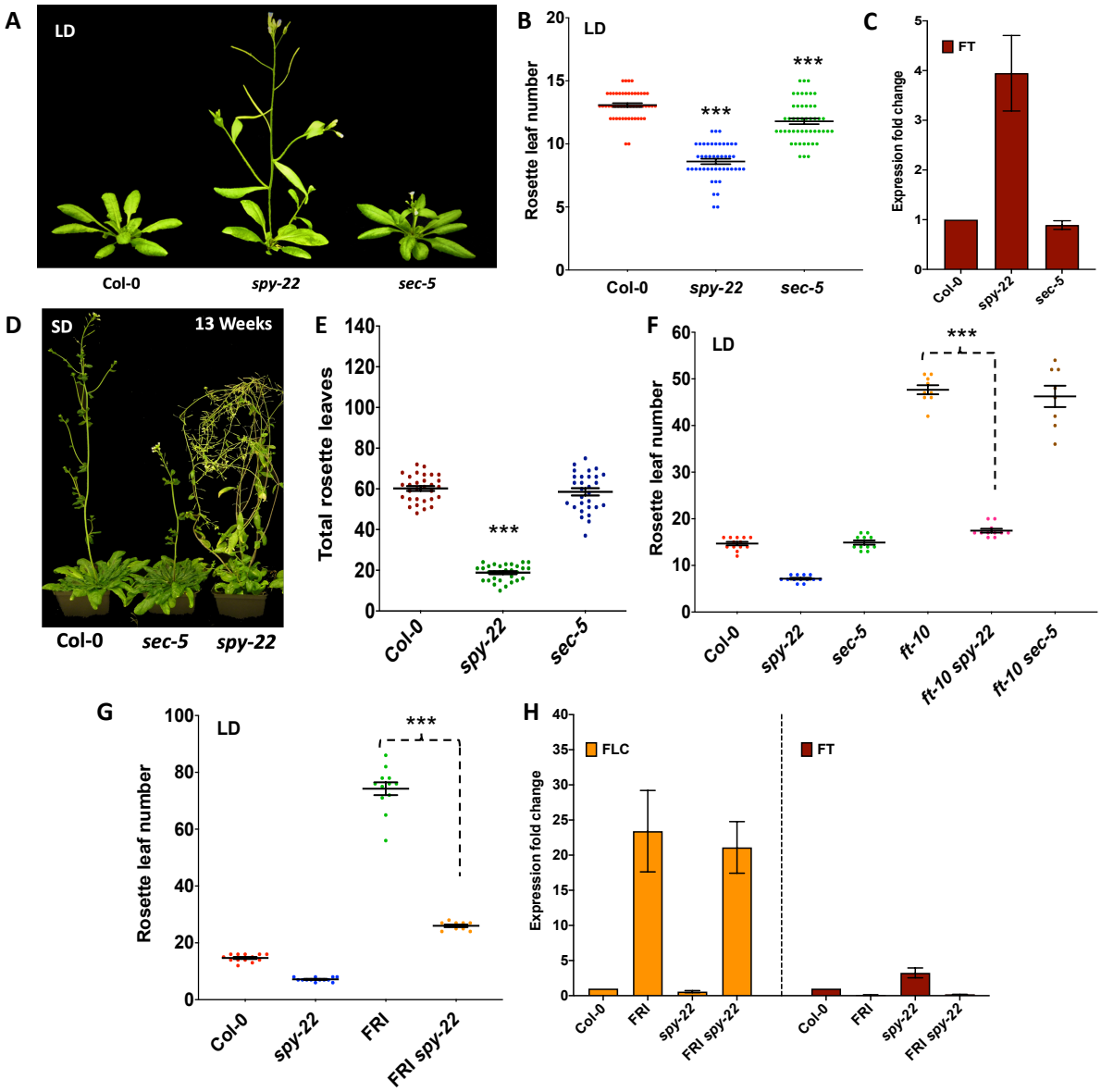

908
909
910
911 **Figure 1. SPY suppresses flowering in long and short photoperiods.**
912 (**A**) Representative pictures of wildtype Col-0, *spy-22* and *sec-5* grown in LD conditions, and
913 **(B)** total rosette leaf numbers of these lines. (**C**) Relative expression levels of *FT* in 10-day old
914 seedlings of *spy-22* and *sec-5* grown in LD conditions. (**D**) Representative pictures of wildtype
915 Col-0, *spy-22* and *sec-5* grown in SD conditions, and **(E)** total rosette leaf numbers of these
916 lines. (**F**) Total rosette leaf numbers of wildtype Col-0, *spy-22, sec-5, ft-10, ft-10 spy-22* and
917 *ft-10 sec-5* grown in LD conditions. **(G)** Total rosette leaf numbers of wildtype Col-0, *spy-22,*
918 Col-0 FRI and FRI *spy-22* grown in LD conditions, and **(H)** relative expression levels of *FLC*
919 and *FT* in 10-day old seedlings of Col-0, *spy-22,* Col-0 FRI and FRI *spy-22* grown in LD
920 conditions.
921 For expression analysis, an average of three biological repeats ± SEM is shown, n > 20. For
922 comparison of rosette leaf numbers, one-way ANOVA with Tukey's multiple comparison was
923 done, n is given in Table 1 (*** $p \leq 0.001$).

924 Figure 2
925

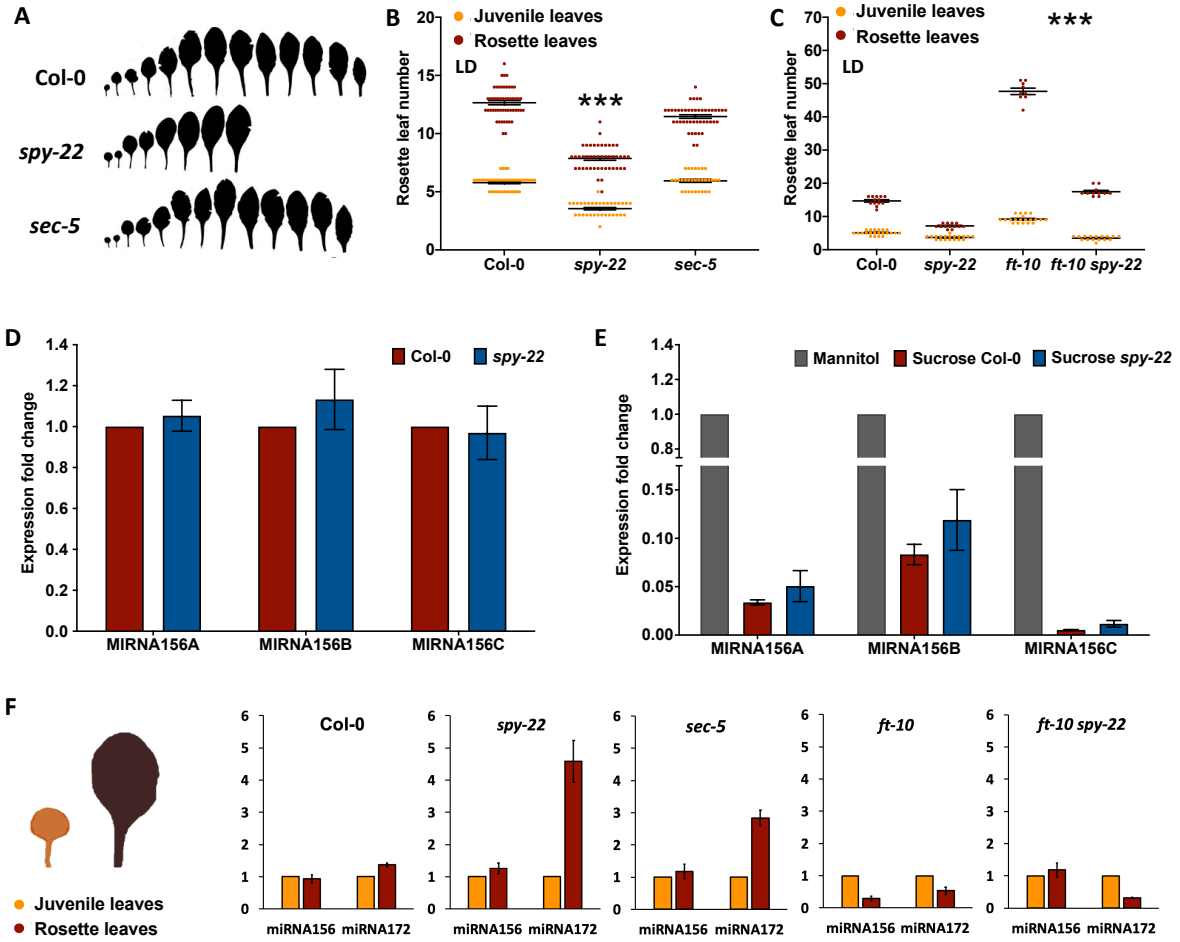

926
927

928 **Figure 2. SPY regulates juvenile to adult phase transitions**

929 (**A**) Leaf scans (left panel) and juvenile and total leaf numbers (right panel) of wildtype Col-0,
930 *spy-22* and *sec-5* grown in LD conditions. One-way ANOVA with Tukey's multiple comparison
931 was done, n is given in Table 2. (*** $p \leq 0.001$, ns: not significant). (**B**) Juvenile and total leaf
932 numbers of wildtype Col-0, *spy-22, ft-10* and *ft-10 spy-22* grown in LD conditions. (**C**) Relative
933 expression levels of primary *miR156a*, *-b* and *-c* in Col-0 and *spy-22* in 5-day old seedlings,
934 an average of three biological repeats +/- SEM is shown, n > 20. **(D)** Relative expression levels
935 of primary *miR156a*, *-b*, and *-c* in Col-0 and *spy-22* in 5-day old seedlings treated with 50 mM
936 sucrose for 24 h. An average of two biological repeats is shown, n > 20. **(E)** Relative
937 expression of mature *miR156* and *miR172* in juvenile and adult leaves of Col-0, *spy-22*, *sec-*
938 *5*, *ft-10* and *ft-10 spy-22*. Representative results of one out of three biological repeats (average
939 ± SD) are shown.
940
941
942
943
944
945
946
947

Figure 3

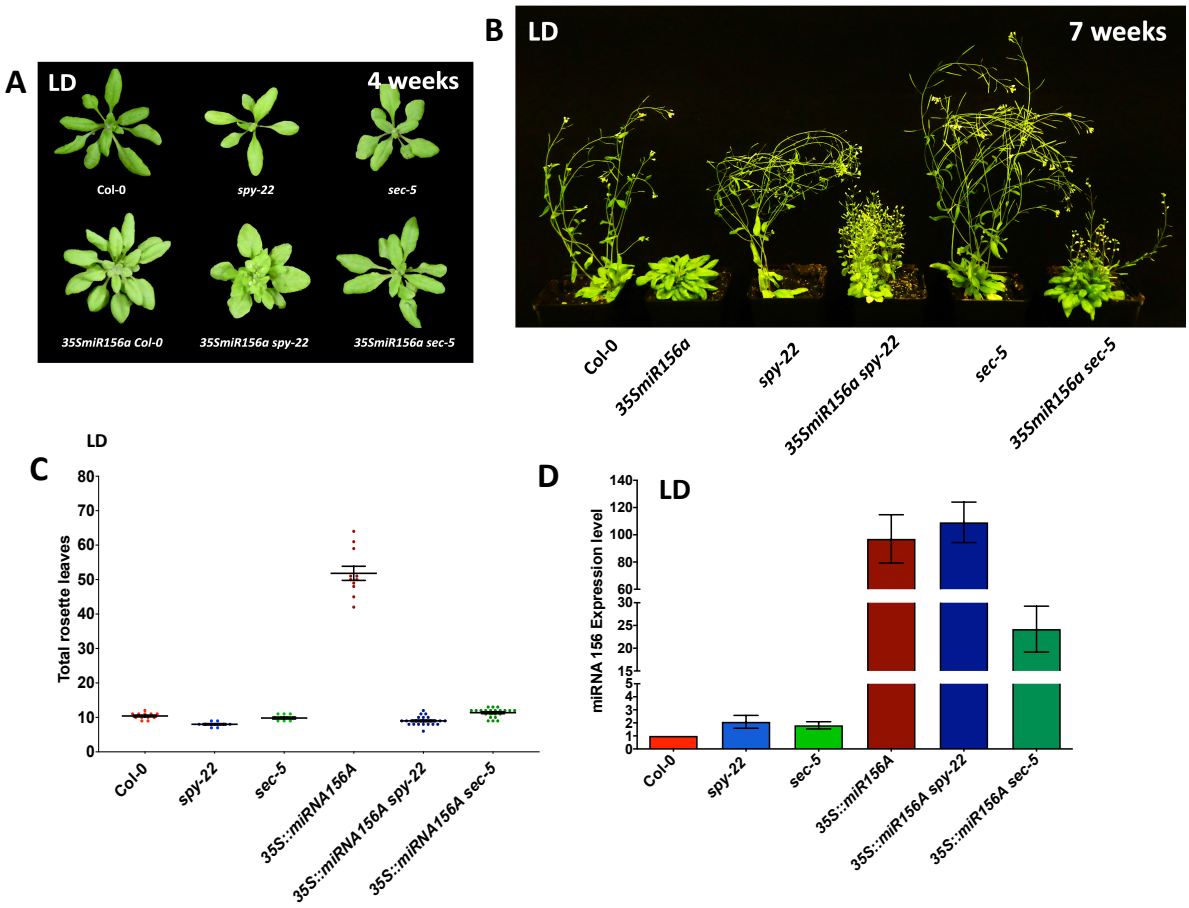

Figure 3. Overexpression phenotypes of miR156 are suppressed in *spy-22* and *sec-5*

(A, B) Representative pictures of 4-week-old (A) and 7-week-old (B) plants of wildtype Col-0, *spy-22* and *sec-5* crossed with *35S::miRNA156a.* **(C)** Total rosette leaves of *35S::miRNA156a* Col-0*, 35S::miRNA156a spy-22* and *35S::miRNA156a sec-5*, n is given in Table 3. **(D)** Relative expression levels of mature *miR156* in juvenile leaves of wildtype Col-0, *spy-22*, *sec-5*, *35S::miRNA156a* Col-0*, 35S::miRNA156a spy-22* and *35S::miRNA156a sec-5*. One biological repeat (average ± SD) is shown.

973 Figure 4
974

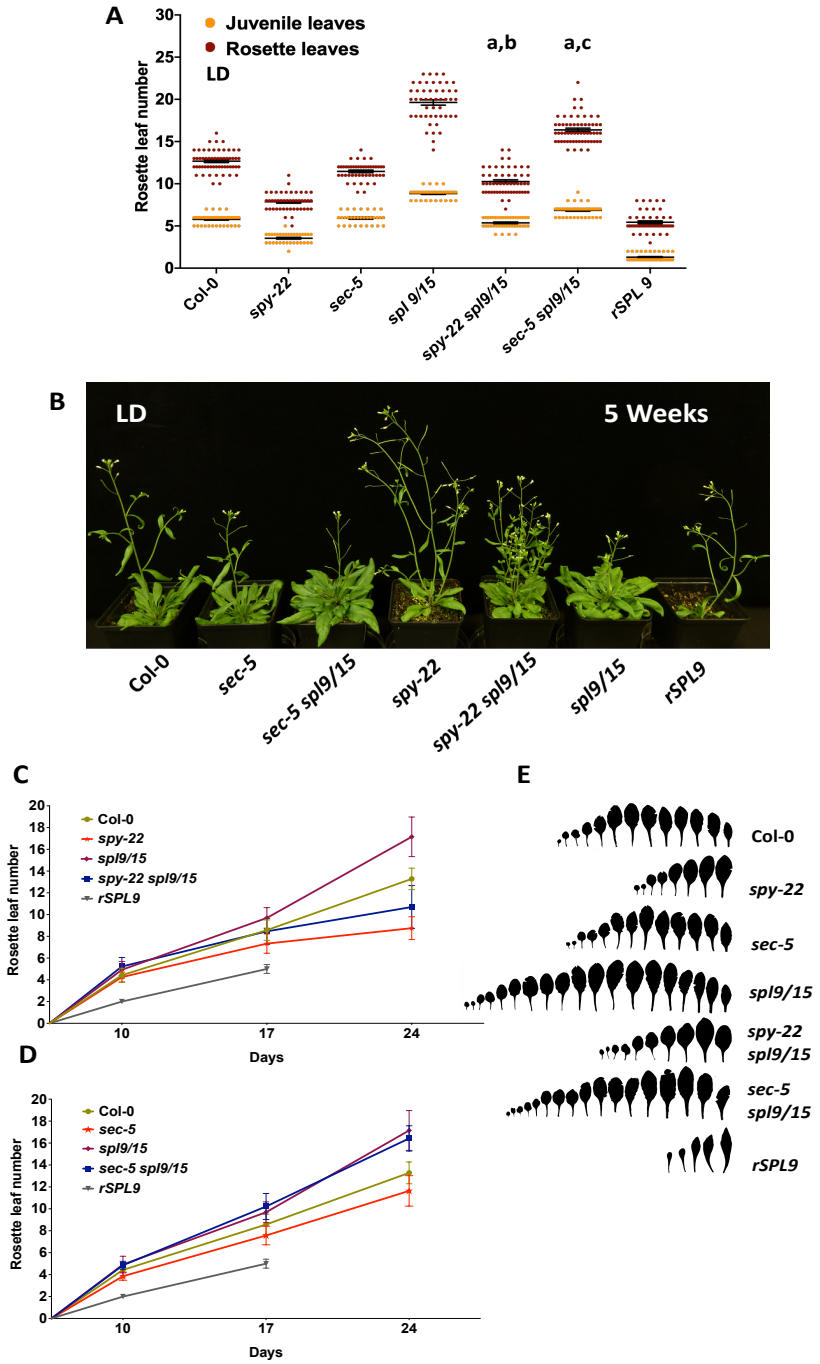

975
976
977 **Figure 4: O-glycosylation represses phase transitions partly via SPL9 and SPL15**
978 (**A**) Juvenile and total rosette leaf numbers of plant lines indicated in the graph, grown in LD
979 conditions. Averages ± SEM are shown. For comparison of rosette leaf numbers, one-way
980 ANOVA with Tukey's multiple comparison was done, n is given in Table 4 ([a] significantly more
981 juvenile and rosette leaves than *spy-22* or *sec-5* (*** $p \leq 0.001$), [b] significantly fewer juvenile
982 and rosette leaves than *spl9-4/15-1* (*** $p \leq 0.001$) [c] significantly fewer juvenile leaves than
983 *spl9-4/15-1* (** $p \leq 0.01$). Full statistical comparison is given in Table 4.
984 **(B)** Representative pictures of 6-week-old plants with leaf numbers shown in (A). **(C,D)**
985 Rosette leaf numbers over time of plants quantified in (A), averages ± SD are given. **(E)** Leaf
986 scans of total rosette leaves of the indicated lines.
987

988 Figure 5

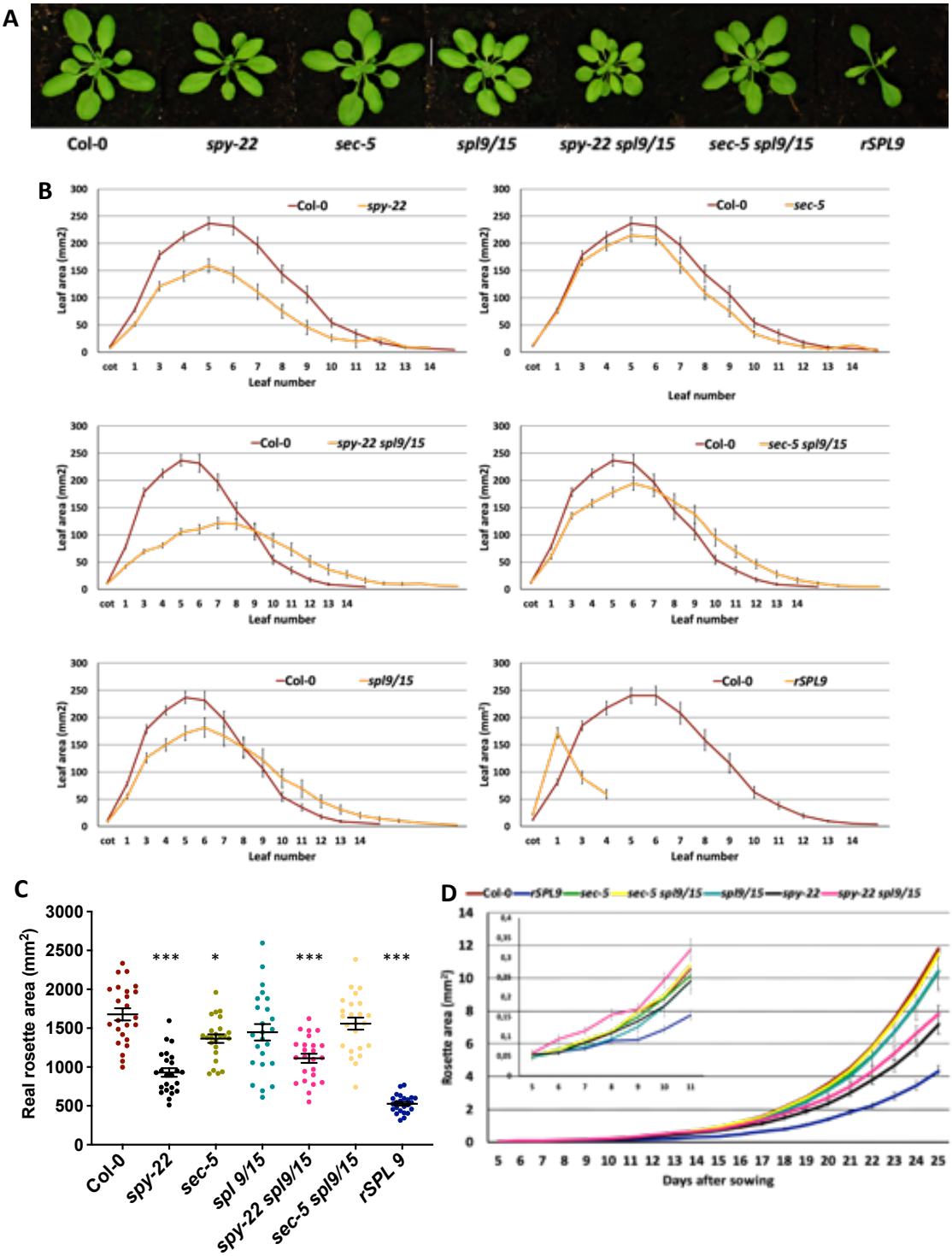

989

990 **Figure 5. SPY and SPL9/SPL15 regulate leaf growth**

991 (**A**) Representative pictures of 25-day-old rosettes of plants used for leaf and rosette area
992 measurements. (**B**) Leaf areas of lines indicated in the graph. Averages ± SEM of three
993 biological repeats using 8 plants per line for each repeat are shown. (**C**) Real rosette area,
994 calculated from the leaf area measurements depicted in (B). For statistical analysis, one-way
995 ANOVA with Tukey's multiple comparison was done, significant differences to the wildtype
996 Col-0 are shown (*** $p \leq 0.001$, * $p \leq 0.05$). (**D**) growth rates of rosette areas (mm^2) of the
997 indicated lines.

998

Figure 6

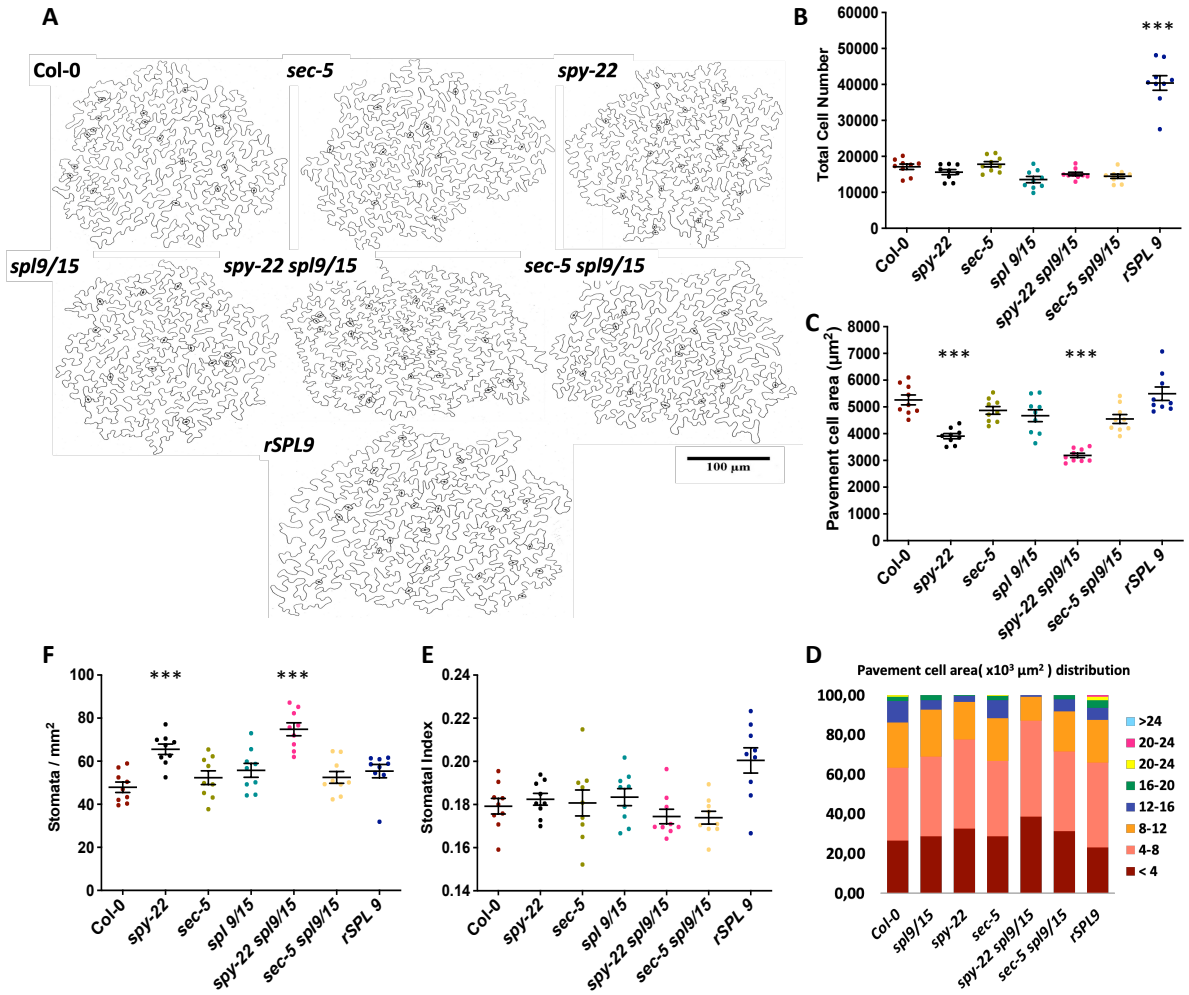

Figure 6. Cellular analysis of *spy-22, sec-5, spl9/15 triple mutants and SPL9::rSPL9:GFP*.

(A) Representative drawings of cell margins of the indicated lines, as used for the analysis of cell numbers, areas, circularity, SI and SD. **(B)** Total epidermal cell number and **(C)** pavement cell area of lines indicated in the graph. **(D)** Distribution of pavement cell area of the indicated lines. **(E)** Stomatal Index (SI) and **(F)** stomata density (SD) of the indicated lines. Averages ± SEM of three biological repeats using 3 plants per line for each repeat are shown (n = 9). For statistical analysis, one-way ANOVA with Tukey's multiple comparison was done, significant differences to the wildtype Col-0 are shown (*** $p \leq 0.001$, * $p \leq 0.05$).

Figure 7

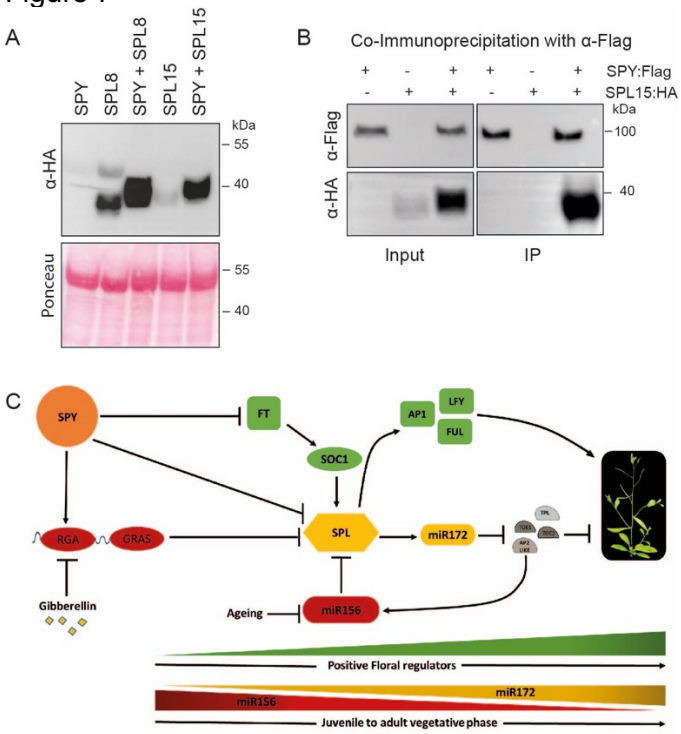

Figure 7. SPY interacts with SPLs.

(**A**) Western Blot of protein extracts from transient expression in *N. benthamiana*, *35S::SPY:Flag*, *35S::SPL8:HA*, *35S::SPL15:HA* single infiltrations, as well as *35S::SPY:Flag*, *35S::SPL8:HA* and *35S::SPY:Flag*, *35S::SPL15:HA* co-infiltration is shown. Protein extracts were blotted and probed with anti HA-antibody to visualize SPL8 and SPL15. **(B)** Samples after co-infiltration of transiently expressed *35S::SPY:Flag* and *35S::SPL15:HA* were used for immunoprecipitation of SPY using an anti-Flag antibody, co-immunoprecipitation of SPL15 is shown with an anti-HA antibody. **(C)** Current working model suggesting a role for O-glycosylation at several levels in the regulation of developmental transitions in *Arabidopsis thaliana*.

1038 Supplemental Figure 1.

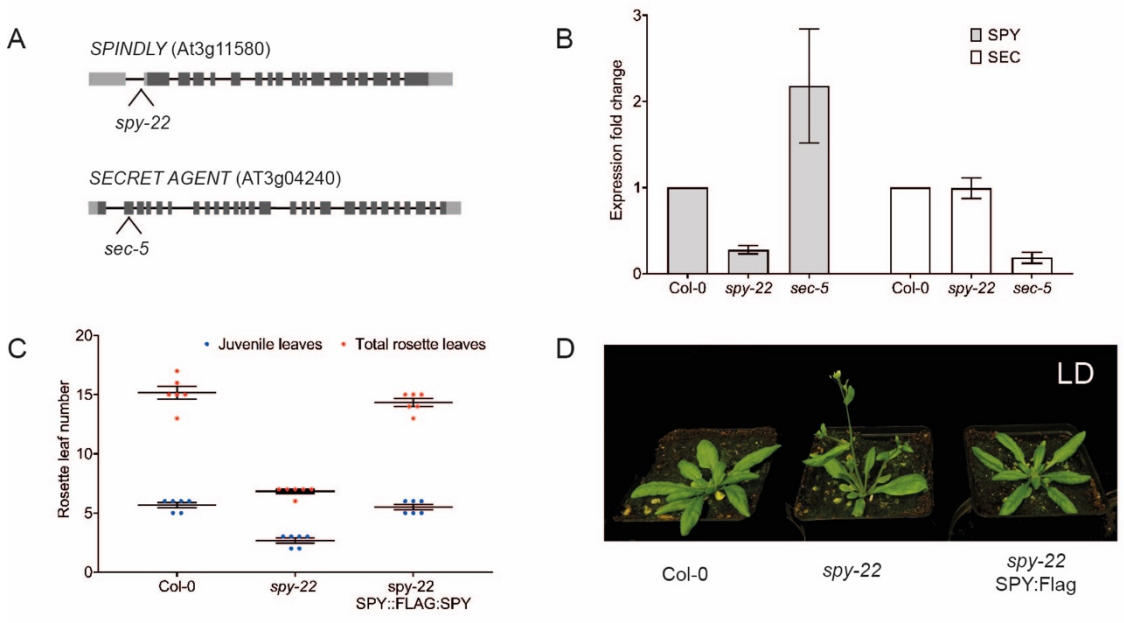

1039

1040 **Supplemental Figure 1. Description of mutant lines *spy-22* and *sec-5***

1041 (**A**) Structure of *SPY* and *SEC*, 5'- and 3'-UTR are shown in light grey and exons in dark grey
1042 boxes, the lines represent introns. The position of the T-DNA insertion in *spy-22*
1043 (SALK_090582) and *sec-5* (SALK_034290) are given. (**B**) Relative expression levels of *SPY*
1044 and *SEC* in *spy-22* and *sec-5 seedlings,* an average of three biological repeats ± SEM is
1045 presented, n > 20. (**C**) Juvenile and total rosette leaf numbers of wildtype Col-0, *spy-22* and
1046 *spy-22 SPY::SPY:Flag* (*SPY:Flag*) grown in LD conditions. (**D**) Representative pictures of
1047 wildtype Col-0, *spy-22,* and *spy-22 SPY::SPY:Flag* (*SPY:Flag*) grown in LD conditions.

1048
1049
1050
1051
1052
1053
1054
1055
1056
1057
1058
1059
1060
1061
1062
1063
1064
1065
1066

1067 Supplemental Figure 2.

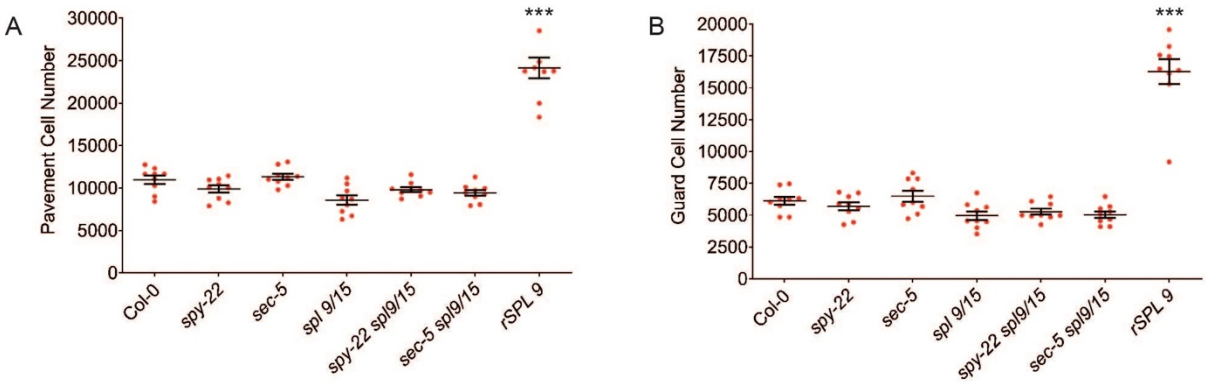

1068
1069 **Supplemental Figure 2.**

1070 (**A**) Pavement and **(B)** guard cell numbers of lines indicated in the graph. Averages ± SEM of
1071 three biological repeats using 3 plants per line for each repeat are shown (n = 9). For statistical
1072 analysis, one-way ANOVA with Tukey's multiple comparison was done, significant differences
1073 to the wildtype Col-0 are shown (*** $p \leq 0.001$).

1074
1075
1076
1077
1078
1079
1080
1081
1082
1083
1084
1085
1086
1087
1088
1089
1090
1091
1092
1093
1094
1095
1096
1097
1098
1099
1100
1101
1102

1103 Supplemental Figure 3

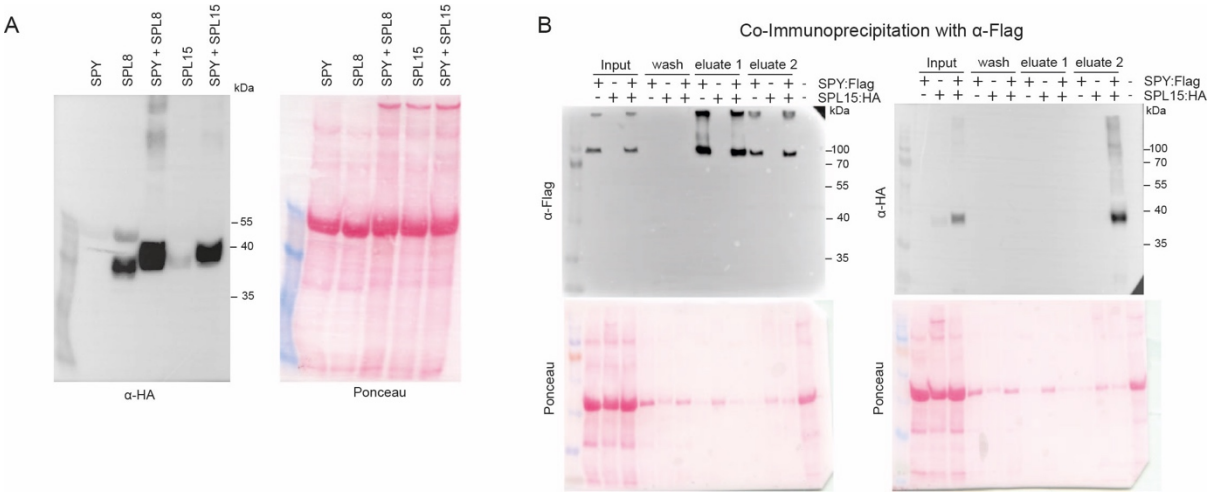

1104
1105
1106 **Supplemental Figure 3. Full membranes of blots shown in Figure 7.**
1107